Application of the Mixed and Hybrid Finite Element Formulations

by

Pratik Rao

in partial fulfillment of the requirements of the degree of

Master of Science

in Aerospace engineering

at Delft University of Technology

Supervised by Marc Gerritsma

Associate Professor,

Department of Aerospace engineering,

Delft University of Technology.

February 16, 2018

Acknowledgements

At the outset, I would like to state that my MSc project has been one of my most challenging and interesting pursuits. I feel proud of this achievement but without the help of many people, this journey would have not been possible.

Firstly, I am extremely thankful and grateful towards my academic supervisor, Dr.ir. Marc Gerritsma who never failed to keep me motivated me during the entire duration of the project. He was always supportive and I thank him for devoting so much of his time in imparting his knowledge to me. He has a great sense of humour which kept the research atmosphere really positive. In addition to this, I would like to thank him, Ir. Liesbeth and Prof. Tim Phillips because without them, my future plans would not be so clear.

The help of PhD students Ir. Yi Zhang and Ir. Varun Jain is well appreciated especially during a crucial time period. They helped me get accustomed to some concepts and saved me time in building the numerical scheme.

I would like to thank my friends Niko, Saurabh and Jaydeep for their support which ensured that I am on track with my coursework. I am extremely grateful to Maria who has always shown belief in me. Her constant love and care made everything a lot easier and instilled a lot of confidence in me. I feel indebted towards Andreas and Maria for their unwavering support since I first met them.

Lastly, I would like to deeply thank my family for their unconditional love and support without whom this beautiful journey would not even have begun. From taking wonderful care of me all through the years to supporting my decision to move abroad, I feel very lucky.

Abstract

Partial Differential Equations (PDEs) are a fundamental tool in modelling various physical phenomena. The lack of closed form solutions in most cases continues to provide a strong incentive to seek stable and consistent numerical methods. This report deals specifically with the mixed and hybrid finite element formulations; ideas that were originally developed in the 1960's for problems in linear elasticity. Hybrid formulations have very attractive properties but are plagued with non-physical singular modes known as Spurious Kinematic Modes (SKMs). This report is devoted to the development of a hybrid scheme in linear elasticity that is free of SKMs. In the scheme, both the stress fields and kinematic fields are treated as primary variables and can hence be obtained together while also satisfying the equilibrium conditions throughout the physical domain. Subsequently, it is shown that optimal convergence is obtained for the stress and displacement fields. A versatile scheme is setup such that it can be solved efficiently by parallelisation of the system. Finally, an idea is mentioned regarding the extension to fluid dynamics.

Contents

List of Figures

Chapter 1

Introduction

Partial Differential Equations (PDEs) are fundamental tools used in modelling several physical phenomena that are based on the strong formulation while the variational formulation is a weak formulation. The latter is based on determining the critical points of a Lagrange functional. Traditionally, this means that the problem is formulated as one in which it is required to minimise a particular functional. Minimisation problems however, are only a subset of the vast branch of variational problems and the study of such problems is known as Calculus of Variations or Variational Calculus (Appendix A). From the formal view point, the problem of minimising a definite integral is considered as a proper domain of variational calculus while the problem of minimising a function forms a part of ordinary calculus, [1]. It is a flexible technique that can be used to determine the extremum and/or critical points of a functional, subject to one or more constraints with the help of Lagrange multipliers. This is known as a constrained optimisation problem that can be solved to yield a Variational Boundary Value Problem (VBVP).

Even if the optimisation problem is analysed to be well-posed, closed-form solutions are usually unavailable. This is why there is a strong incentive to build numerical models using approximate methods such as finite difference, finite volume and finite element formulations. Variational analysis is the heart of finite element formulations, [2] and the main motivation of this report is the investigation of the mixed and hybrid finite element approaches that were originally formulated in the 1960s to tackle prob-

lems in linear elasticity and finite element methods, [3]. After a brief comparison of the mixed and the direct (or primal) finite element formulation for the Poisson's equation, majority of the report deals with the development of a hybrid finite element scheme for $\mathbb{R}^2$ problems in linear elasticity. Linear elasticity is chosen as the focal point due to the vast and rich literature for finite element methods in this field. All hybrid formulations lead to the introduction of singular kinematic modes in the system known as Spurious Kinematic Modes (SKMs), [4]. These modes lead to a singular matrix which in turn doesn't permit a unique solution. Despite these problems, hybrid schemes are highly sought after due to many attractive properties that will be discussed in this report. Based on the observations, we pose the main research question as,

Can we develop a finite element method for linear elasticity that is free of Spurious Kinematic Modes (SKMs)?

We hope to have a positive answer to this research question by the thorough analysis of the numerical scheme once it is setup.

Chapter 2

Finite element formulation

In most cases, a closed form solution is not available for a given problem even if it is analysed to be well-posed. Hence, approximate solutions are sought; with Finite element formulations being one of the many means of seeking these solutions. The PDE by itself is known as the *strong formulation* and while the VBVP is the *weak formulation*; the latter being the point of departure for the finite element formulations, [2]. However, instead of posing the problem on an infinite dimensional Hilbert space, it is solved on the subspace of this infinite dimensional space; i.e. a finite dimensional space. And here, the Ritz-Galerkin approach is applied, [5]. A domain Ω in $\mathbb{R}^n$ is divided into subdomains called *elements* that have a specific geometry. Subsequently, a space S of functions in Ω are approximated by polynomial basis functions that are defined for each element and satisfy the boundary conditions. Every element is equipped with points known as *nodes* which must (at the very least) be present at the vertices of each element. The basis functions are constructed in such a way that they are non-zero for a very small part of Ω, making them an attractive prospect for computations. The nice property of the finite element formulation is that if more elements N are taken into account, the quality of the approximate solution improves. Some types of finite element formulations include the primal or direct formulation, mixed formulation and hybrid formulation.

2.1 Example

When we think of Poisson's equation, we usually think of it as a PDE from which we can derive the VBVP. However, the VBVP can also be obtained from the minimisation of a functional. Consider the functional $\mathcal{J}(u)$ governing a smooth and closed domain Ω bounded by Γ,

$$\mathcal{J}(u) \;=\; \frac{1}{2}\int_\Omega |\nabla u|^2 \;\mathrm{d}\Omega \;-\; \int_\Omega f u \;\mathrm{d}\Omega \qquad u \in H_0^1(\Omega),\;\; f \in L^2(\Omega)\;. \tag{2.1}$$

The objective is to find u such that the function is minimised. For this, we use the perturbation $u+\epsilon\tilde{u}$ in the functional and equate the Gâteaux variation to zero in order to find the minimum of the functional. Note that $\tilde{u} \in H_0^1(\Omega)$ is arbitrary. We have,

$$\frac{d}{d\epsilon}\mathcal{J}(u+\epsilon\tilde{u})\bigg|_{\epsilon=0} \;=\; 0\;,$$

resulting in,

$$\int_\Omega \nabla u : \nabla\tilde{u} \;\mathrm{d}\Omega \;=\; \int_\Omega f\tilde{u} \;\mathrm{d}\Omega \qquad \forall\tilde{u} \in H_0^1(\Omega)\;. \tag{2.2}$$

Equation (2.2) is the Variational Boundary Value Problem (VBVP). Sometimes, there may not be a minimisation problem so the VBVP is a more fundamental formulation. Note that the VBVP can also be obtained from the strong PDE form of the Poisson's equation,

$$-\Delta u \;=\; f\;, \tag{2.3}$$

subject to the Dirichlet BC $u = 0$ on the boundary Γ. If we take the inner product of equation (2.3) with test function $\tilde{u}$,

$$-\int_\Omega \Delta u \;\tilde{u} \;\mathrm{d}\Omega \;=\; \int_\Omega f\tilde{u} \;\mathrm{d}\Omega\;,$$

At this stage, we can have $\tilde{u} \in L^2(\Omega)$ but when we apply integration by parts and Gauss divergence theorem,

$$\int_\Omega \nabla u : \nabla \tilde{u} \ \mathrm{d}\Omega \ - \underbrace{\int_\Gamma \frac{du}{dn} \ \tilde{u} \ \mathrm{d}\Gamma}_{=0} \ = \ \int_\Omega f\tilde{u} \ \mathrm{d}\Omega \quad \forall \tilde{u} \in H_0^1(\Omega) \ ,$$

we get VBVP as shown in equation (2.2) and therefore $\tilde{u} \in H_0^1(\Omega)$,

$$\int_\Omega \nabla u : \nabla \tilde{u} \ \mathrm{d}\Omega \ - \ \int_\Omega f\tilde{u} \ \mathrm{d}\Omega \ = \ 0 \quad \forall \tilde{u} \in H_0^1(\Omega) \ . \tag{2.4}$$

Note that the boundary integral vanishes because $\tilde{u} \in H_0^1(\Omega)$ and hence $\tilde{u}|_\Gamma = 0$. Also, u minimises the functional in equation (2.1); that is,

$$u = \inf_{u \in H_0^1(\Omega)} \ \mathcal{J}(u) \ . \tag{2.5}$$

2.2 Primal formulation

The primal finite element formulation is the most standard technique in finite elements. In $\mathbb{R}^1$, the approximate solution for field u is of the form $u^h = \sum_{i=1}^N u_i \phi_i^u(x)$ where $\phi_i^u(x)$ is the basis function and coefficients u_i are the unknown coefficients to be determined. Using the example in section 2.1, if we take $\tilde{u} = v$, equation (2.4) becomes,

$$\int_\Omega \nabla u : \nabla v \ d\Omega \ - \ \int_\Omega f v \ d\Omega \ = \ 0 \quad \forall v \in H_0^1(\Omega) \ , \tag{2.6}$$

which we pose on a finite dimensional space $S^h \subset H_0^1(\Omega)$,

$$\int_\Omega \nabla u^h : \nabla v^h \ d\Omega \ - \ \int_\Omega f v^h \ d\Omega \ = \ 0 \quad \forall v^h \in S^h \ . \tag{2.7}$$

This is known as the **primal finite element formulation**. To get the discrete form, substitute the basis functions for $u^h \in S^h$ and $v^h \in S^h$,

$$\sum_{j=1}^N v_j \underbrace{\int_\Omega \nabla \phi_j^v \nabla \phi_i^u(x) d\Omega}_{\mathcal{M}_{ji}} \ \sum_{i=1}^N u_i \ = \ \sum_{j=1}^N v_j \underbrace{\int_\Omega f\phi_i \ d\Omega}_{\mathcal{F}_i} \ ,$$

resulting in the matrix system,

$$\mathcal{M}\mathscr{U} = \mathcal{F} \ , \tag{2.8}$$

where $\mathscr{U} = [u_1, u_2, \ldots, u_i, \ldots u_n]$ are the coefficients that become known by solving the above equation. The matrix $\mathcal{M}$ must be non-singular for unique $\mathscr{U}$. Once $\mathscr{U}$ is known, it is substituted in the expansion u^h and we have our approximate solution. Note that *numerical integration* is used in most cases in order to evaluate the matrices $\mathcal{M}$ and $\mathcal{F}$. Now that the basic idea is explained, results are presented for a domain $\Omega = [0\ 1]$ with Dirichlet boundary conditions. The exact solution that satisfies the Poisson's equation subject to the boundary conditions is given by,

$$u = \sin(\pi x) \ . \tag{2.9}$$

The basis function that was used is the piecewise linear (hat) function, [6], governed by the property,

$$\phi_i^u(x_j) = \delta_{ij} = \begin{cases} 1, & \text{if } i = j. \\ 0, & \text{otherwise.} \end{cases}$$

$$\phi_i^u(x) = \begin{cases} \dfrac{x - x_i}{h_i}, & \text{if } x_{i-1} \leq x < x_i \ . \\ \dfrac{x_{i+1} - x}{h_i}, & \text{if } x_i \leq x < x_{i+1} \ . \\ 0, & \text{otherwise} \ . \end{cases}$$

Results are presented for a relatively coarse mesh containing just 10 elements and a sufficiently fine mesh containing 60 elements in Figure 2.1.

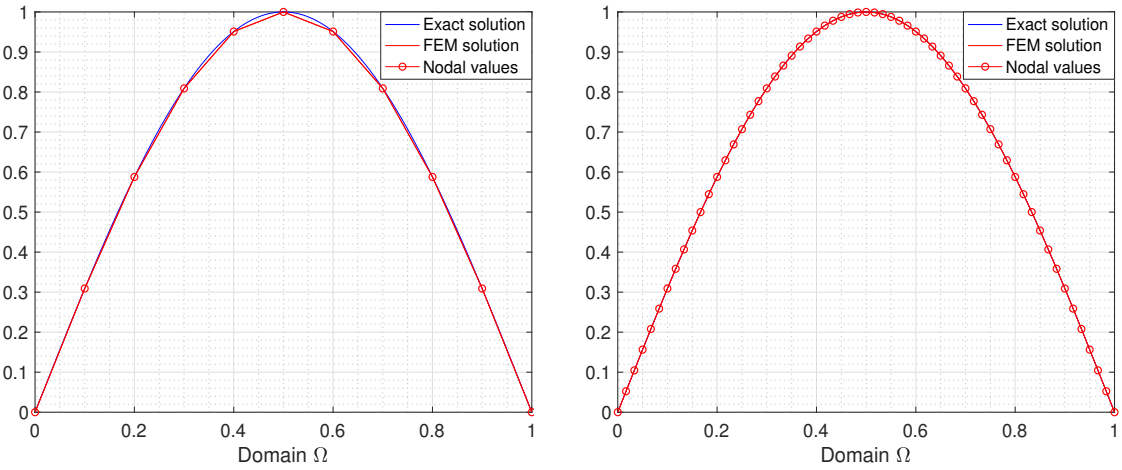

(a) Coarse mesh (b) Fine mesh

Figure 2.1: Validation of the primal formulation

The error ϵ of the method is measured by computing the infinity norm for the same parameters in Figure 2.2 for a specific coarse and fine mesh. The infinity norm is given by,

$$\|\epsilon\|_\infty = \max \left| u - u^h \right| \ . \tag{2.10}$$

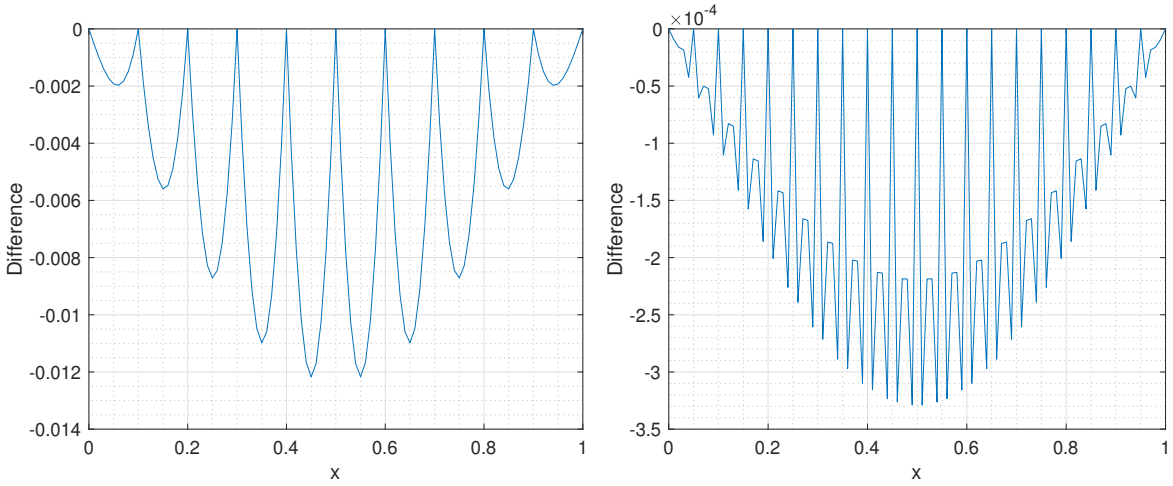

(a) Coarse mesh (b) Fine mesh

Figure 2.2: Error variation in the domain

For a coarse mesh involving just 10 elements, the linear nature of the solution can be seen seen very clearly. The jump of the solution from one element to another is visible.

However, making the mesh finer with 60 elements, the exact solution cannot even be seen because it is superimposed (almost) 'exactly' by the numerical solution. Once again, the difference in error is stark by just increasing the number of elements. We now move to another finite element formulation called the mixed formulation.

2.3 Mixed formulation

The mixed formulation was first used in around 1960s to describe finite element methods (FEM) where *both* stress and displacement variables were approximated as primary variables, [7]. A mixed formulation is obtained by factoring the original set of equations into a system of first-order systems. After this conversion, a VBVP is constructed and discretised using the same procedure used for primal formulation in section 2.2.

An attempt is made to derive the mixed formulation of equation (2.3). Let's define a variable $q \in H(\text{div}; \Omega)$ such that,

$$\begin{aligned} q &= \nabla u \ , \\ \nabla \cdot q &= -f \ , \end{aligned} \tag{2.11}$$

over the entire domain Ω with $u \in L^2_0(\Omega)$. Multiplying the first equation of system (2.11) with $\tilde{q} \in H(\text{div}; \Omega)$ and integrating over Ω,

$$\int_\Omega q \cdot \tilde{q} \ \mathrm{d}\Omega \ = \ \int_\Omega \nabla u \cdot \tilde{q} \ \mathrm{d}\Omega \quad \forall \tilde{q} \in H(\text{div}; \Omega) \ ,$$

$$\int_\Omega q \cdot \tilde{q} \ \mathrm{d}\Omega \ - \ \underbrace{(\tilde{q} \ u \cdot \hat{n})\Big|_\Gamma}_{=\ 0} \ + \ \int_\Omega u \nabla \cdot \tilde{q} \ \mathrm{d}\Omega \ = \ 0 \quad \forall \tilde{q} \in H(\text{div}; \Omega) \ .$$

Hence, the following equation when represented in matrix form will satisfy the Dirichlet boundary condition $u|_\Gamma = 0$,

$$\int_\Omega q \cdot \tilde{q} \ \mathrm{d}\Omega \ + \ \int_\Omega u \ (\nabla \cdot \tilde{q}) \ \mathrm{d}\Omega \ = \ 0 \quad \forall \tilde{q} \in H(\text{div}; \Omega) \ . \tag{2.12}$$

Multiplying the second equation of system (2.11) with $\tilde{u} \in L^2_0(\Omega)$,

$$\int_\Omega (\nabla \cdot q)\ \tilde{u}\ \mathrm{d}\Omega \ = \ -\int_\Omega f\tilde{u}\ \mathrm{d}\Omega \quad \forall \tilde{u} \in L^2_0(\Omega)\ . \tag{2.13}$$

Equations (2.12) and (2.13) can also be obtained by taking Gâteaux variations with respect to the functional, [8],

$$\mathcal{I}(q,u) \ = \ \int_\Omega \frac{1}{2}|q|^2 - u(\nabla \cdot q)\ \mathrm{d}\Omega \ + \ \int_\Omega fu\ \mathrm{d}\Omega, \tag{2.14}$$

over $H(\mathrm{div};\Omega) \times L^2(\Omega)$. Variationally, this is a *saddle point* problem. That is, the solution to the problem is,

$$(q,u) = \inf_{q \in H(\mathrm{div};\Omega)} \sup_{u \in L^2(\Omega)} \mathcal{I}(q,u). \tag{2.15}$$

Performing a finite element method over a saddle point problem is known as the mixed finite element formulation. However, to perform the procedure of finite elements, we must move to a subspace $Q^h \subset H(\mathrm{div};\Omega)$, $V^h \subset L^2(\Omega)$ and find the solution (q^h, u^h) on the space $Q^h \times V^h$. To get an appropriate and physically meaningful solution in the above formulation, the function spaces Q^h and V^h must be *different*, [8]. We choose piecewise linear basis functions for q and piecewise constant functions for u.

2.3.1 Basis functions

An element e_i is defined between the nodes x_i and x_{i+1} and is associated with one or more basis functions. For a compatible discretisation, they must be chosen wisely as discussed.

Piecewise linear functions for the finite dimensional representation of q (and $\tilde{q}$)

Each element is associated with two basis functions $\phi_i(x)$ and $\phi_{i+1}(x)$ such that,

$$\begin{aligned} \phi_i^q(x) &= 1 - \frac{x}{h_i} \\ \phi_{i+1}^q(x) &= \frac{x}{h_i} \ , \end{aligned} \tag{2.16}$$

where $h_i = x_{i+1} - x_i$ is the step size. Since q^h is expanded in the form of linear basis functions (approximately), we have,

$$q^h = \sum_{i=1}^{n} q_i \phi_i^q(x) \ ,$$

where n is the number of nodes in the physical domain.

Piecewise constant functions for the finite dimensional representation of u (and $\tilde{u}$)

These functions are defined are defined over each element. Edge functions are used which have the property,

$$\phi_i^u(x) = \frac{1}{h_i} \ .$$

Since they are defined over each element, u can be expanded (approximately) as,

$$u^h = \sum_{i=1}^{n-1} u_i \phi_i^u(x) \ .$$

2.3.2 Discrete form

Now that the basis functions are derived, we can write these equations in matrix form. To do this, we isolate each term of the equations (2.12) and (2.13) and simplify them.

The final system is,

$$\begin{pmatrix} \mathcal{A} & \mathcal{B}^T \\ \mathcal{B} & 0 \end{pmatrix} \begin{bmatrix} \mathscr{Q} \\ \mathscr{U} \end{bmatrix} = \begin{bmatrix} 0 \\ -\mathcal{F} \end{bmatrix} , \tag{2.17}$$

with $\mathscr{Q} = [q_1, q_2, \ldots, q_i, \ldots q_n]$ and $\mathscr{U} = [u_1, u_2, \ldots, u_i, \ldots u_n]$ contain the coefficients of the basis function expansions for u^h and q^h. A_{ji}, an element of the square matrix $\mathcal{A}$ is defined as,

$$\int_\Omega \phi_j^q(x)\phi_i^q(x) \ d\Omega,$$

and B_{ji}, an element of the non-square $\mathcal{B}$ is defined as,

$$\int_\Omega \phi_j^u(x)\phi_i^{q'}(x) \ d\Omega,$$

and B_{ji}^T, an element of $\mathcal{B}^T$ is defined as,

$$\int_\Omega \phi_j^{q'}(x)\phi_i^u(x) \ d\Omega.$$

Again, for unique solutions for u^h and q^h, the LHS matrix has to be non-singular. Also note that even here, numerical integration is performed to evaluate the LHS and RHS matrices. As mentioned earlier, the choice of basis functions is crucial, if the hat function that was used in the primal formulation is used to represent q^h, the discretisation is clearly incompatible as seen in Figure 2.3. However, for the same number of elements, we have a compatible disrectisation if we use the linear basis functions in equation (2.16) as shown in Figure 2.4. The exact solutions u, q are shown in blue while the numerical solution u^h, q^h are shown in red. Note that the since the exact solution is given by equation (2.9), its gradient q is given by,

$$q = \pi \cos(\pi x) \ . \tag{2.18}$$

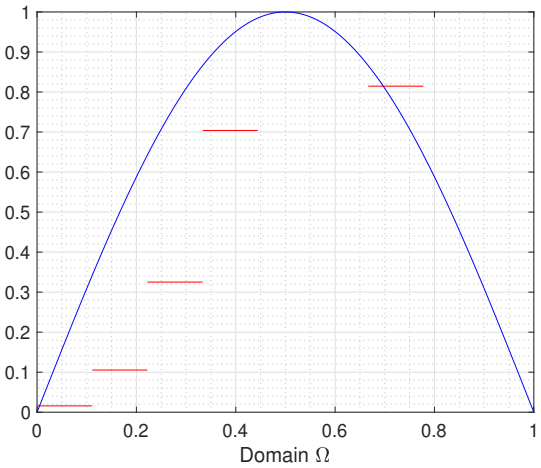

(a) Comparison of u and u^h

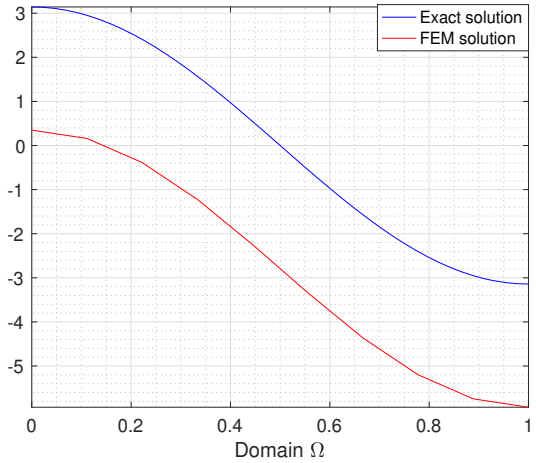

(b) Comparison of q and q^h

Figure 2.3: Incompatible discretisation

Now that we know the choice of basis functions leading to a compatible discretisation, we can make the mesh finer. The results look much nicer now in Figure 2.5 where we have the solution for both u^h and q^h. The numerical solution q^h is superimposed on the exact solution q due to the high accuracy.

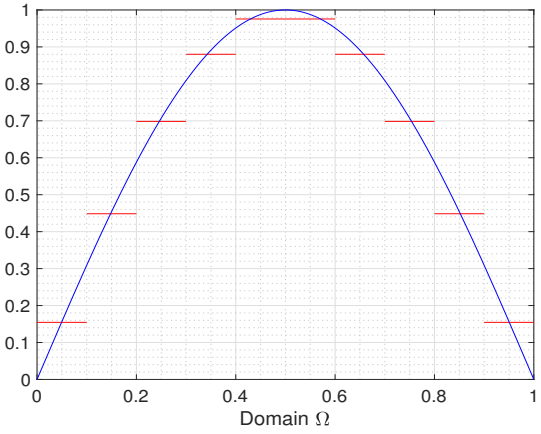

(a) Comparison of u and u^h

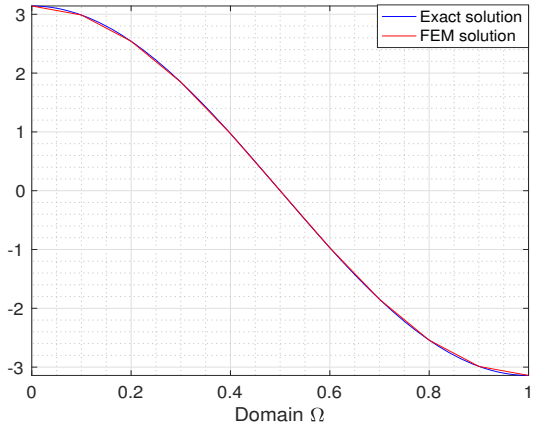

(b) Comparison of q and q^h

Figure 2.4: Compatible discretisation

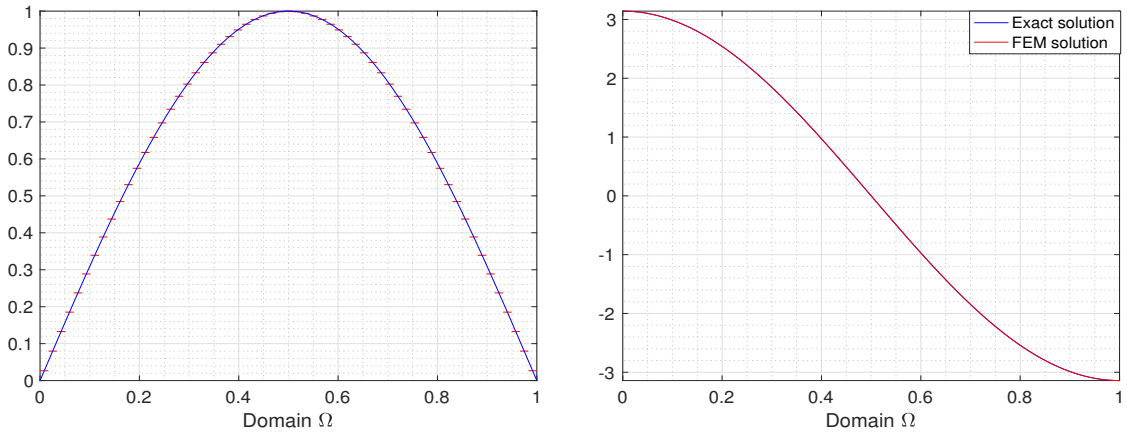

(a) Comparison of u and u^h

(b) Comparison of q and q^h

Figure 2.5: Results from a fine mesh with 60 elements

2.4 Remarks

In the mixed formulation, we can obtain the solution of 2 primary variables u^h and its gradient, q^h. In the primal formulation, we get only one result u^h and all other results must be obtained *a posteriori*. The gradient of u^h should be obtained by differentiating the solution, which entails a loss of accuracy, [7]. Also, the primal formulation requires the space $H_0^1(\Omega)$ while the mixed formulation uses $u^h \in L^2(\Omega)$ and $q^h \in H(\text{div}; \Omega)$. In the test case discussed here, we have the solution for u^h in the form of continuous curve in the primal formulation; and in the form of piecewise constant lines in the mixed formulation. Another important point to be noted is that in the primal formulation,

$$u^h = \inf_{u^h \in S^h} \mathcal{J}(u^h), \tag{2.19}$$

and in the mixed formulation,

$$(q^h, u^h) = \inf_{q^h \in Q^h} \sup_{u^h \in V^h} \mathcal{I}(q, u). \tag{2.20}$$

which are basically the finite dimensional versions of equations (2.5) and (2.15) respectively. However, the former is a minimisation problem, the latter is a saddle point

problem. An important aspect after finding the approximate solution of a chosen finite element scheme is an error analysis. We know that in the primal formulation, u was the exact solution and u^h was the approximate one. The error was computed using the infinity norm in equation (2.10). In complicated test cases, where u is unknown, the error has to be estimated. In addition to this, we must determine the rate of convergence as well. This is where functional analysis is important; choosing the function space for solutions is crucial and has to be a normed space (this is another reason why Banach and Hilbert spaces are important in FEM). Just like the Euclidean norm that defines the length of a vector, there are norms used to determine values of functions. The maximum norm on a space $\mathbb{X}$ containing bounded, continuous functions is given by, [2],

$$\|u\|_{\mathbb{X}} = \max\{|u(x)|, \ \ \forall x \in \Omega\}.$$

Since the finite element formulation uses a subspace $\mathbb{X}^h$ of $\mathbb{X}$, the error estimate becomes,

$$\|u - u^h\|_{\mathbb{X}} \leq Ah^{-p},$$

where A, p are positive constants that are independent of h. The equation shows that increasing h; i.e. increasing the space $\mathbb{X}^h$ **improves** the approximation. This is why the finer mesh in both formulations showed much better results: $\|u - u^h\| \to 0$ as $h \to \infty$. For example, the rate of convergence p for the primal formulation is determined as shown in Figure 2.6.

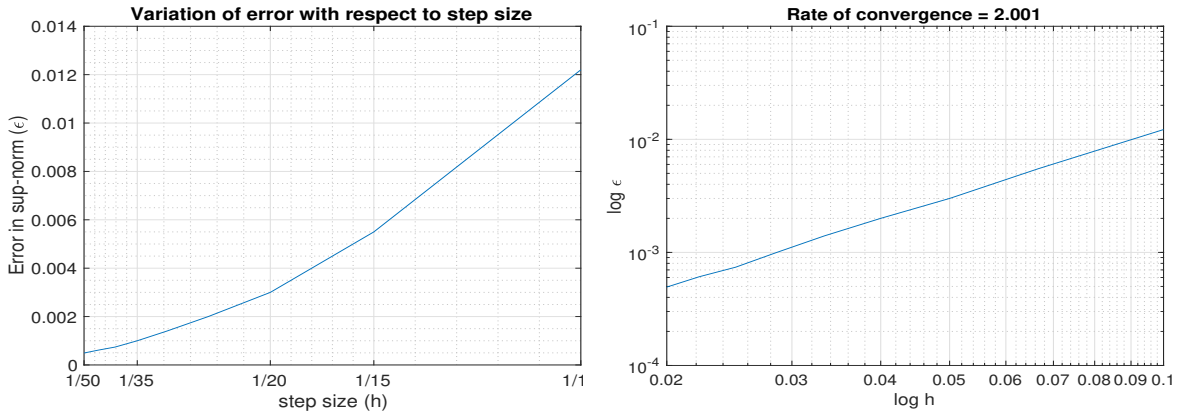

(a) Error in the infinity norm

(b) Rate of convergence from log-log plot

Figure 2.6: Error analysis with respect to step size for Primal formulation

The procedure and results were shown for the VBVP of the Poisson's equation in $\mathbb{R}^1$. The advantages were discussed for the mixed formulation. However, there are disadvantages such as carefully determining the function spaces for the unknown variables. When we increase the number of dimensions, the number of unknown variables naturally increases thereby increasing the complexity of the problem. In addition to this, for the study of physical phenomena such as linear elasticity in solid mechanics and incompressible flows in fluid dynamics, there are more relations involved. This, once again leads to an increase in complexity of the problem. Now that the mixed formulation has been investigated, we move to discussing hybrid finite element formulation for linear elasticity problems in $\mathbb{R}^2$.

Chapter 3

Hybrid formulation

The hybrid finite element formulation is based on domain decomposition methods allied to duality. In any such formulation, the variational principle is dependent on how the domain Ω is partitioned into subdomains; but independent of any discretisation [5]. In many finite element formulations tested for elasticity, the equilibrium of forces is satisfied only at the *nodes*. There are usually discrepancies in satisfying the equilibrium within a given element and at boundaries between elements thereby violating Newton's third law of motion, [9]. To circumvent this problem, hybrid ideas were formulated to decouple the problem into separate problems for each subdomain Ω_i and impose continuity at the interfaces between the subdomains with the help of additional variables (Lagrange multipliers). The equations and variables involved in structural problems are very geometrical, [10] and hence, if variables are expanded with respect to geometrical structures such as lines and surfaces in addition to just nodes, the formulation is more physical, [11]. An advantage of the hybrid formulation is that it is not too complicated to implement. However, all hybrid formulations lead to singularities in the algebraic model. Basically, the results are non-physical and are generated with respect to kinematic properties such as displacement, velocity, rotation, etc. These are known as Spurious Kinematic Modes (SKM). [12] provides exhaustive literature on how these SKM's work, where they may be expected in the geometry, how their behaviour affects the results of numerical experiments, etc. Since most schemes do have SKMs, certain techniques have been developed to remove SKMs

such as the application of a stress potential or by direct approximations of the stress field in elements, [9]. Other techniques involve the use of super elements, [13] but they are mostly difficult to implement, [14].

In this chapter, we introduce some relations in linear elasticity and conservation laws. Subsequently, we build a hybrid scheme that can be applied to linear elasticity problems in $\mathbb{R}^2$. Basis functions are assumed for the stresses; while displacements may be prescribed on the (entire or parts of the) boundary. The special aspect of these stress expansions is that the coefficients of the expansion are surface forces (integrated stress field) so they have physical meaning. Since the stresses are expanded in terms of forces distributed over surfaces of the element, continuous stress fields are produced over element boundaries. The formulation is based on the principal of minimisation of the complementary energy, [15], subject to the constraints that linear and angular momentum equilibrium is established in the entire physical domain and not just at the nodes of elements.

3.1 Linear elasticity

Linear elasticity is a field of solid mechanics that is characterised by 3 main field variables namely, displacement $\boldsymbol{u}$, strain $\underset{\approx}{\epsilon}$ and stress $\underset{\approx}{\sigma}$. It analyses deformable bodies which can be under the influence of external surface loading and internal body forces. There are several kind of loading such as a point loads, uniformly distributed loads and variably distributed loads. A typical kind of body force is the self weight of a body under which a body can deform even without external forces. In $\mathbb{R}^2$, let us introduce the following nomenclature,

$$\boldsymbol{u} \;=\; [u,\;\; v]^T \;,$$

$$\boldsymbol{\epsilon} \;=\; [\epsilon_{xx},\;\; \epsilon_{yx},\;\; \epsilon_{xy},\;\; \epsilon_{yy}]^T \;,$$

$$\boldsymbol{\sigma} \;=\; [\sigma_{xx},\;\; \sigma_{yx},\;\; \sigma_{xy},\;\; \sigma_{yy}]^T \;,$$

where $\boldsymbol{u}$, $\boldsymbol{\sigma}$ and $\boldsymbol{\epsilon}$ are expressed in vector form. In tensor form,

$$\underset{\approx}{\epsilon} = \begin{pmatrix} \epsilon_{xx} & \epsilon_{yx} \\ \epsilon_{xy} & \epsilon_{yy} \end{pmatrix} ,$$

$$\underset{\approx}{\sigma} = \begin{pmatrix} \sigma_{xx} & \sigma_{yx} \\ \sigma_{xy} & \sigma_{yy} \end{pmatrix} .$$

The strain and rotation are governed by *compatibility* relations,

$$\epsilon_{ij} = \frac{1}{2}\left(\frac{\partial u_i}{\partial x_j} + \frac{\partial u_j}{\partial x_i}\right) = \epsilon_{ji} , \tag{3.1}$$

$$\omega_{ij} = \frac{1}{2}\left(\frac{\partial u_j}{\partial x_i} - \frac{\partial u_i}{\partial x_j}\right) = -\omega_{ji} .$$

Therefore,

$$\epsilon_{ij} = \frac{\partial u_j}{\partial x_i} + \omega_{ji} . \tag{3.2}$$

Note that these relations hold for small values of strain and rotation. Finally, we have the *constitutive* equations to relate stress and strain, which is related through the compliance tensor C_{ijkl},

$$\epsilon_{ij} = C_{ijkl}\sigma_{kl} . \tag{3.3}$$

Traction vectors $\boldsymbol{t}$ are related to the components of the stress tensor $\underset{\approx}{\sigma}$ as follows,

$$\begin{pmatrix} \sigma_{xx} & \sigma_{yx} \\ \sigma_{xy} & \sigma_{yy} \end{pmatrix} \begin{bmatrix} n_x \\ n_y \end{bmatrix} = \begin{bmatrix} t_x \\ t_y \end{bmatrix} ,$$

or in Einstein notation, $\boldsymbol{t}_i = \sigma_{ji}\boldsymbol{n}_j$. Here $\boldsymbol{n}$ refers to the unit normal.

3.1.1 Conservation Laws

Under static equilibrium, if $\boldsymbol{t}$ is the traction vector, $\boldsymbol{f}$ is the body force density, conservation of linear momentum is given by, [16],

$$\int_A \boldsymbol{t} \ \mathrm{d}A \ + \ \int_V \boldsymbol{f} \ \mathrm{d}V \ = \ 0 \ , \tag{3.4}$$

Applying divergence theorem, we now have,

$$\int_A \sigma_{ji} n_j \ \mathrm{d}A \ = \ \int_V \frac{\partial \sigma_{ij}}{\partial x_i} \ \mathrm{d}V \ = \ -\int_V f_j \ \mathrm{d}V \ .$$

If this holds for all volumes, the following holds over Ω,

$$\frac{\partial \sigma_{ij}}{\partial x_i} \ = \ -f_j \ , \tag{3.5}$$

or equivalently as,

$$\nabla \cdot \boldsymbol{\sigma} \ = \ -\boldsymbol{f} \ . \tag{3.6}$$

Under static equilibrium, if $\boldsymbol{r}$ is the position vector with respect to the origin, conservation of angular momentum is given by, [17],

$$\int_A (\boldsymbol{r} \times \boldsymbol{t}) \ \mathrm{d}A \ + \ \int_V (\boldsymbol{r} \times \boldsymbol{f}) \ \mathrm{d}V \ = \ 0 \ . \tag{3.7}$$

Working with the first integral,

$$\int_A \epsilon_{ijk} \ x_j t_k \ \mathrm{d}A = \int_A \epsilon_{ijk} \ x_j \sigma_{mk} n_m \ \mathrm{d}A \ ,$$

which is converted into a volume integral using the divergence theorem,

$$\int_V \frac{\partial}{\partial x_m} (\epsilon_{ijk} \ x_j \sigma_{mk}) \ \mathrm{d}V \ = \ \int_V \epsilon_{ijk} \left(\delta_{jm} \sigma_{mk} + x_j \frac{\partial \sigma_{mk}}{\partial x_m} \right) \ \mathrm{d}V \ ,$$

where ϵ_{ijk} is the Levi-Cevita tensor and δ_{jm} is the Kronecker delta function. Considering $\mathbb{R}^2$, simplifying further results in,

$$\int_V \frac{\partial}{\partial x}\left(x\sigma_{xy} - y\sigma_{xx}\right) + \frac{\partial}{\partial y}\left(x\sigma_{yy} - y\sigma_{yx}\right) \ \mathrm{d}V \ ,$$

Now the second integral,

$$\int_V (\boldsymbol{r} \times \boldsymbol{f}) \ \mathrm{d}V \ = \ \int_V \left(xf_y - yf_x\right) \ \mathrm{d}V \ .$$

Therefore, we have,

$$\int_V \frac{\partial}{\partial x}\left(x\sigma_{xy} - y\sigma_{xx}\right) + \frac{\partial}{\partial y}\left(x\sigma_{yy} - y\sigma_{yx}\right) \ \mathrm{d}V \ = \ \int_V \left(yf_x - xf_y\right) \ \mathrm{d}V \ .$$

If this holds for all volumes, the following holds over Ω,

$$\frac{\partial}{\partial x}\left(x\sigma_{xy} - y\sigma_{xx}\right) + \frac{\partial}{\partial y}\left(x\sigma_{yy} - y\sigma_{yx}\right) + \left(xf_y - yf_x\right) \ = \ 0 \ . \tag{3.8}$$

Simplifying,

$$\sigma_{xy} - \sigma_{yx} + x\underbrace{\left(\frac{\partial \sigma_{xy}}{\partial x} + \frac{\partial \sigma_{yy}}{\partial y}\right)}_{-f_y} - y\underbrace{\left(\frac{\partial \sigma_{xx}}{\partial x} + \frac{\partial \sigma_{yx}}{\partial y}\right)}_{-f_x} + \left(xf_y - yf_x\right) \ = \ 0 \ , \tag{3.9}$$

thereby leading to the important result, the symmetry of the stress tensor,

$$\sigma_{xy} - \sigma_{yx} \ = \ 0 \ . \tag{3.10}$$

Either equation (3.8) or (3.10) can be enforced as a constraint in the discrete setting. In this project, calculations were performed for both equations but the latter is preferred while performing simulations. This is because, there are lesser terms involved. As a result, the matrix is more sparse and hence the system is more computationally efficient.

3.2 Variational principles

As has been discussed earlier, finite element formulations are applied to variational problems that usually involve finding critical points of energy functionals. In solid mechanics, there are several variational principles such as principle of minimum potential energy, the principle of minimum complementary energy, the Hellinger–Reissner variational principle, and the Hu–Washizu variational principle, [15]. This report will deal with the formulation of stress hybrid elements and hence deals with the minimisation of the complementary energy, [15],

$$\mathcal{J}(\boldsymbol{\sigma}) \;=\; \frac{1}{2}\int_{\Omega} \boldsymbol{\sigma}^T C \boldsymbol{\sigma} \;\mathrm{d}\Omega \;-\; \int_{\Gamma_u} \boldsymbol{t}^T \bar{\boldsymbol{u}} \;\mathrm{d}\Gamma \;, \tag{3.11}$$

where T represents the transpose operator, $\bar{\boldsymbol{u}}$ are the known displacements prescribed on parts of the boundary Γ_u and C is the compliance tensor, [9], given by,

$$C \;=\; \frac{1}{E}\begin{pmatrix} 1 & 0 & 0 & -\nu \\ 0 & (1+\nu) & 0 & 0 \\ 0 & 0 & (1+\nu) & 0 \\ -\nu & 0 & 0 & 1 \end{pmatrix}, \tag{3.12}$$

where E is the Young's modulus and ν is the Poisson's ratio. Initially, when we build the scheme, we do not consider prescribed displacements so the boundary integral over Γ_u is neglected. In addition to this, even body force density $\boldsymbol{f}$ terms are dropped but can be reintroduced whenever needed. In order to add more constraints to the functional $\mathcal{J}(\boldsymbol{\sigma})$; Lagrange multipliers are required. The Lagrange multipliers used to impose conservation of linear momentum and angular momentum turn out to be displacement and rotation fields respectively. The use of kinematic variables to impose dynamic constraints has been done before in, [9, 18]. Due to the addition of constraints, we now have a Lagrangian functional,

$$\mathcal{L}(\boldsymbol{\sigma}, \boldsymbol{u}, \boldsymbol{\omega}) \;=\; \frac{1}{2}\int_{\Omega} \boldsymbol{\sigma}^T C \boldsymbol{\sigma} \;\mathrm{d}\Omega \;+\; \int_{\Omega} \boldsymbol{u}^T \left[\nabla \cdot \boldsymbol{\sigma}\right] \mathrm{d}\Omega \;+\; \int_{\Omega} \boldsymbol{\omega}^T \boldsymbol{R} \boldsymbol{\sigma} \;\mathrm{d}\Omega \;, \tag{3.13}$$

where $\boldsymbol{R} = [0, -1,\ 1,\ 0]$ has been used to impose symmetry of stress tensor at the continuous level. The stationary points of equation (3.13) solve the constitutive equation (3.3) subject to the conservation of momentum (3.6), (3.10). This can be proven if we perturb the stress: $\boldsymbol{\sigma} + \epsilon\tilde{\boldsymbol{\sigma}}$, the displacement field: $\boldsymbol{u} + \alpha\tilde{\boldsymbol{u}}$ and the rotation field as $\boldsymbol{\omega} + \beta\tilde{\boldsymbol{\omega}}$. Here, all fields involving the $\sim$ are arbitrary. We take the Gâteaux variation (Appendix A) with respect to each of the variables and equate them to zero. The first variation is,

$$\left.\frac{\partial \mathcal{L}\left(\boldsymbol{\sigma} + \epsilon\tilde{\boldsymbol{\sigma}},\ \boldsymbol{u} + \alpha\tilde{\boldsymbol{u}},\ \boldsymbol{\omega} + \beta\tilde{\boldsymbol{\omega}}\right)}{\partial \boldsymbol{\epsilon}}\right|_{\epsilon=\alpha=\beta=0} = 0\,,$$

which implies,

$$\int_\Omega \tilde{\boldsymbol{\sigma}}^T C\boldsymbol{\sigma}\ \mathrm{d}\Omega\ +\ \int_\Omega \boldsymbol{u}^T(\nabla\cdot\tilde{\boldsymbol{\sigma}})\ \mathrm{d}\Omega\ +\ \int_\Omega \boldsymbol{\omega}^T\boldsymbol{R}\tilde{\boldsymbol{\sigma}}\ \mathrm{d}\Omega\ =\ 0\,,\qquad \forall\tilde{\boldsymbol{\sigma}} \in [H(\mathrm{div};\Omega)]^2\,. \tag{3.14}$$

Applying integration by parts to the second term and simplifying,

$$\int_\Omega \tilde{\boldsymbol{\sigma}}^T C\boldsymbol{\sigma}\ \mathrm{d}\Omega - \int_\Omega \tilde{\boldsymbol{\sigma}}^T(\nabla\boldsymbol{u})\ \mathrm{d}\Omega + \int_{\Gamma_t} \underbrace{\tilde{\boldsymbol{\sigma}}\cdot\boldsymbol{n}}_{=\tilde{\boldsymbol{t}}}\boldsymbol{u}\ \mathrm{d}\Gamma + \int_\Omega \boldsymbol{\omega}^T\boldsymbol{R}\tilde{\boldsymbol{\sigma}}\ \mathrm{d}\Omega\ =\ 0\,,\qquad \forall\tilde{\boldsymbol{\sigma}} \in [H(\mathrm{div};\Omega)]^2\,.$$

The boundary integral disappears because the variations $\tilde{\boldsymbol{t}} = 0$. The infinitesimal rotation vector is just $[\omega_{xy}]$. This can be obtained using $\frac{1}{2}(\nabla\times\boldsymbol{u})$ and are the components of the full rotation vector, [19]. Coupling this fact with equation (3.2), we have,

$$\boldsymbol{\epsilon} = \nabla\boldsymbol{u} - \boldsymbol{R}^T\boldsymbol{\omega}\,.$$

As a result of this, the integral equation is simplified to,

$$\int_\Omega \tilde{\boldsymbol{\sigma}}^T\left(C\boldsymbol{\sigma} - \boldsymbol{\epsilon}\right)\ \mathrm{d}\Omega\ =\ 0.\qquad \forall\tilde{\boldsymbol{\sigma}} \in [H(\mathrm{div};\Omega)]^2\,, \tag{3.15}$$

as a result of the first variation. Next we have,

$$\left.\frac{\partial \mathcal{L}\left(\boldsymbol{\sigma} + \epsilon\tilde{\boldsymbol{\sigma}},\ \boldsymbol{u} + \alpha\tilde{\boldsymbol{u}},\ \boldsymbol{\omega} + \beta\tilde{\boldsymbol{\omega}}\right)}{\partial \boldsymbol{\alpha}}\right|_{\epsilon=\alpha=\beta=0} = 0\,,$$

which implies,

$$\int_{\Omega} \tilde{\boldsymbol{u}}^T (\nabla \cdot \boldsymbol{\sigma}) \ \mathrm{d}\Omega \ = \ 0 \quad \forall \tilde{\boldsymbol{u}} \in [L^2(\Omega)]^2 \ . \tag{3.16}$$

Taking the final variation,

$$\left. \frac{\partial \mathcal{L} \left(\boldsymbol{\sigma} + \epsilon \tilde{\boldsymbol{\sigma}}, \ \boldsymbol{u} + \alpha \tilde{\boldsymbol{u}}, \ \boldsymbol{\omega} + \beta \tilde{\boldsymbol{\omega}} \right)}{\partial \boldsymbol{\beta}} \right|_{\epsilon = \alpha = \beta = 0} \ = \ 0 \ ,$$

which implies,

$$\int_{\Omega} \tilde{\boldsymbol{\omega}}^T \boldsymbol{R} \boldsymbol{\sigma} \ \mathrm{d}\Omega \ = \ 0 \quad \forall \tilde{\boldsymbol{\omega}} \in L^2(\Omega) \ . \tag{3.17}$$

Equations (3.15) shows that it imposes (3.3) in the L^2 sense. Therefore, the stationary points of equation (3.13) solve the constitutive equation (3.3) subject to the conservation of momentum (3.6), (3.10).

3.3 Finite element scheme

The stress hybrid formulation is based on the same variational problem (3.13) but is posed on a smaller space; that is on a finite dimensional subspace. The finite dimensional representations of $\boldsymbol{\sigma}$, $\boldsymbol{u}$ and $\boldsymbol{\omega}$ are written in terms of their individual components with superscript h. For now, body force density terms are neglected for the sake of convenience but they can be introduced in the schemes as and when it is required.

3.3.1 Single element

Before applying hybrid ideas, it is convenient to create a scheme for a single element defined by a closed domain $\Omega = [-1 \ \ 1]^2$ in $\mathbb{R}^2$ with the origin at $(0, \ 0)$. We want to expand the basis functions for the stress components in terms of surface forces over

the element. Low order polynomial expansions will be derived after which, they are directly substituted into each of the terms of equation (3.13). The element defined over Ω is split into two volumes [1], each for the X configuration and the Y configuration as shown in Figure 3.2 and 3.3. This way, linear momentum equilibrium can be enforced separately for the forces in the X and Y direction. The stress components in the X direction are σ_{xx} and σ_{yx}. It can be seen that there are 3 degrees of freedom (dof) along the X direction and 1 dof along the Y direction for the approximate normal stress σ^h_{xx}. For this reason, $\sigma^h_{xx} \in \mathbb{P}^{2,0}$; that is, the polynomial will have *quadratic* variation in X as shown in Figure 3.1 and is constant along in Y.

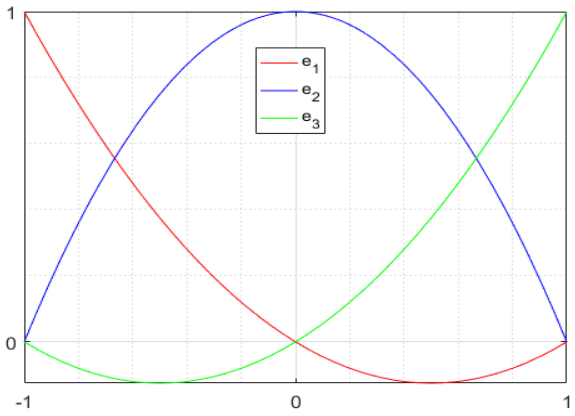

Figure 3.1: Quadratic polynomial expansions

The quadratic polynomials shown in Figure 3.1 are given by,

$$e_1 = \frac{1}{2}x(x-1) ,$$

$$e_2 = (1-x^2) ,$$

$$e_3 = \frac{1}{2}x(x+1) .$$

which have the property that $e_i(x_i) = 1$. Each of these expansions correspond to the 3 dof's. Along Y, edge functions are used which have the property that the definite

[1] This idea was proposed by Ir. Yi Zhang, PhD candidate, Aerospace engineering, Delft University of Technology.

integral of a (constant, c) function along the edge of the element is = 1. Since the limits are -1 to 1, the edge function is just $\frac{1}{2}$,

$$\int_{-1}^{1} c \; \mathrm{d}y \;\; = \;\; 1 \implies c = \frac{1}{2} \; .$$

The edge functions are combined with the quadratic polynomials to yield the expansion polynomials. Therefore, we have,

$$\sigma^h_{xx}(x,y) \;\; = \;\; T^1_{xx}\frac{1}{4}x(x-1) \;\; + \;\; T^2_{xx}\frac{1}{2}(1-x^2) \;\; + \;\; T^3_{xx}\frac{1}{4}x(x+1) \; , \tag{3.18}$$

where the expansion coefficients actually represent the surface forces since,

$$\int_{-1}^{1} \sigma^h_{xx}(-1,y) \; \mathrm{d}y \;\; = \;\; T^1_{xx} \; ,$$

is the integrated stress (hence, surface force) along the left edge $x = -1$. These forces for the X-configuration are shown in Figure 3.2.

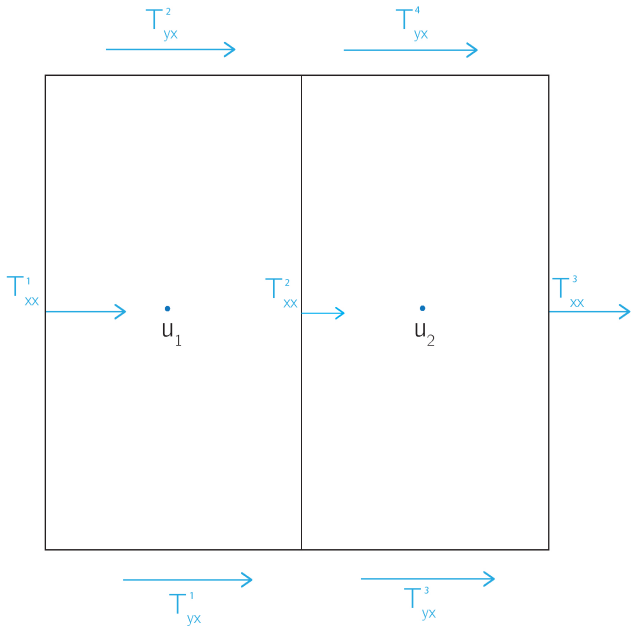

Figure 3.2: Single element with 2 volumes; X configuration

The next stress component σ_{yx} is accompanied with 2 dof in each of the X and Y direction which implies that there must be a linear variation in both X and Y for the

approximation; that is, $\sigma^h_{yx} \in \mathbb{P}^{1,1}$. Using the same property as before, the linear polynomial for the upper edge is $\frac{1}{2}(1+y)$ for the lower edge is $\frac{1}{2}(1-y)$. Along X, edge functions are used which have the property that the definite integral of a (linear) function *only* along the part of the element (where the surface force acts) is = 1 (otherwise, zero). Since the limits are -1 to 0 first and then 0 to 1, we have separate edge functions. For the sides corresponding to forces T^1_{yx} and T^2_{yx}, the expansion is $\left(\frac{1}{2} - x\right)$ since,

$$\begin{aligned} \int_{-1}^{0} \left(\frac{1}{2} - x\right) \, \mathrm{d}x &= 1 \,, \\ \int_{0}^{1} \left(\frac{1}{2} - x\right) \, \mathrm{d}x &= 0 \,. \end{aligned}$$

For the sides corresponding to forces T^3_{yx} and T^4_{yx}, the expansion is $\left(\frac{1}{2} + x\right)$ since,

$$\begin{aligned} \int_{-1}^{0} \left(\frac{1}{2} + x\right) \, \mathrm{d}x &= 0 \,, \\ \int_{0}^{1} \left(\frac{1}{2} + x\right) \, \mathrm{d}x &= 1 \,. \end{aligned}$$

Combining the edge functions and linear expansions, we have our shear stress expansion,

$$\begin{aligned} \sigma^h_{yx}(x,y) &= T^1_{yx}\frac{1}{4}(1-2x)(1-y) + T^2_{yx}\frac{1}{4}(1-2x)(1+y) \\ &+ T^3_{yx}\frac{1}{4}(1+2x)(1-y) + T^4_{yx}\frac{1}{4}(1+2x)(1+y) \,. \end{aligned} \tag{3.19}$$

where superscripts for the forces are **not exponents**. The same procedure must be repeated for the Y-configuration in Figure 3.3,

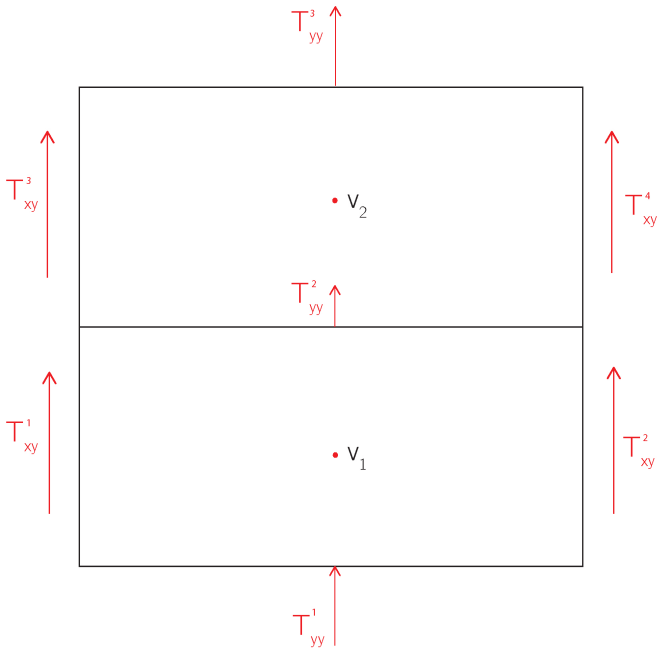

Figure 3.3: Single element with 2 volumes; Y configuration

The approximate stress expansions in the Y direction are given by,

$$\sigma^h_{yy}(x,y) \;=\; T^1_{yy}\frac{1}{4}y(y-1) \;+\; T^2_{yy}\frac{1}{2}(1-y^2) \;+\; T^3_{yy}\frac{1}{4}y(y+1)\;, \tag{3.20}$$

$$\begin{aligned}\sigma^h_{xy}(x,y) \;=\; & T^1_{xy}\frac{1}{4}(1-x)(1-2y) \;+\; T^2_{xy}\frac{1}{4}(1+x)(1-2y) \\ & +\; T^3_{xy}\frac{1}{4}(1-x)(1+2y) \;+\; T^4_{xy}\frac{1}{4}(1+x)(1+2y)\;,\end{aligned} \tag{3.21}$$

where $\sigma^h_{yy} \in \mathbb{P}^{\,0,2}$ and $\sigma^h_{xy} \in \mathbb{P}^{\,1,1}$. Now that the stress expansions have been derived, conservation of linear momentum is applied in X,

$$\frac{\partial \sigma^h_{xx}}{\partial x}+\frac{\partial \sigma^h_{yx}}{\partial y} = \left[T^2_{xx}-T^1_{xx}+T^2_{yx}-T^1_{yx}\right]\frac{1}{4}(1-2x)+\left[T^3_{xx}-T^2_{xx}+T^4_{yx}-T^3_{yx}\right]\frac{1}{4}(1+2x) = 0\;,$$

which means that linear momentum can be satisfied in the space $\mathbb{P}^{\,1,0}$. Similarly, for the Y direction,

$$\frac{\partial \sigma^h_{xy}}{\partial x}+\frac{\partial \sigma^h_{yy}}{\partial y} = \left[T^2_{xy}-T^1_{xy}+T^2_{yy}-T^1_{yy}\right]\frac{1}{4}(1-2y)+\left[T^4_{xy}-T^3_{xy}+T^3_{yy}-T^2_{yy}\right]\frac{1}{4}(1+2y) = 0\;,$$

linear momentum can be satisfied in the space $\mathbb{P}^{\,0,1}$. Noting that $\frac{1}{4}(1-2x)$ and $\frac{1}{4}(1+2x)$ are linearly independent,

$$T^2_{xx} - T^1_{xx} + T^2_{yx} - T^1_{yx} \;=\; 0 \quad \text{and} \quad T^3_{xx} - T^2_{xx} + T^4_{yx} - T^3_{yx} \;=\; 0\,, \tag{3.22}$$

(in each of the volumes) for the X-direction and due to the linear independence of $\frac{1}{4}(1-2y)$ and $\frac{1}{4}(1+2y)$,

$$T^2_{xy} - T^1_{xy} + T^2_{yy} - T^1_{yy} \;=\; 0 \quad \text{and} \quad T^4_{xy} - T^3_{xy} + T^3_{yy} - T^2_{yy} \;=\; 0\,, \tag{3.23}$$

(in each of the volumes) for the Y-direction. This is a good result since linear momentum can be conserved in terms of the expansion coefficients; the forces. The displacement field $\boldsymbol{u}^h$ has two components u^h and v^h that impose the the linear momentum equilibrium in the X and Y direction respectively. Taking a look at Figure 3.2 and 3.3 shows the coefficients u^1, u^2, v^1 and v^2 of the expansions. Due to the presence of 2 dof in one direction and 1 dof in the direction perpendicular to this, there will be a linear variation in the first direction and constant in the second direction. This is why u^h is taken to be linear in X and v^h is taken to be linear in Y; $u^h \in \mathbb{P}^{\,1,0}$ and $v^h \in \mathbb{P}^{\,0,1}$. It is convenient to expand it over Gauss points for the ease in performing numerical integration through Gaussian quadrature, [20]. The basis functions are,

$$\begin{aligned} u^h(x,y) \;&=\; u^1\frac{1}{2}\left(1-x\sqrt{3}\right) \;+\; u^2\frac{1}{2}\left(1+x\sqrt{3}\right)\,, \\ v^h(x,y) \;&=\; v^1\frac{1}{2}\left(1-y\sqrt{3}\right) \;+\; v^2\frac{1}{2}\left(1+y\sqrt{3}\right)\,. \end{aligned}$$

For 2 integration points, the Gauss points are $(-\frac{1}{\sqrt{3}}, \frac{1}{\sqrt{3}})$ and the weights $w_i = 1$. Next, we move on to conserving angular momentum, where we do not explicitly impose symmetry of the stress tensor for now. When calculations are performed, if we eliminate the terms involving conservation of linear momentum, we automatically impose symmetry of stress tensor,

$$\sigma^h_{yx} - \sigma^h_{xy} \;=\; 0\,. \tag{3.24}$$

Note that $\sigma^h_{xy}, \sigma^h_{yx} \in \mathbb{P}^{1,1}$ so this condition can hold in the discrete setting. The symmetry of the stress tensor is imposed by the rotation function $\boldsymbol{\omega}^h$ given by,

$$\begin{aligned}\boldsymbol{\omega}^h(x,y) &= \omega^1\frac{1}{4}(1-x\sqrt{3})(1-y\sqrt{3}) + \omega^2\frac{1}{4}(1-x\sqrt{3})(1+y\sqrt{3}) \\ &+ \omega^3\frac{1}{4}(1+x\sqrt{3})(1-y\sqrt{3}) + \omega^4\frac{1}{4}(1+x\sqrt{3})(1+y\sqrt{3})\,.\end{aligned} \tag{3.25}$$

which is linear in both X and Y due to the presence of 2 dof each in X and Y. Note that the picture is not to scale and the ω_i's are located at the Gauss points $(x_i, y_j) = \left[\left(-\frac{1}{\sqrt{3}}, -\frac{1}{\sqrt{3}}\right), \left(-\frac{1}{\sqrt{3}}, \frac{1}{\sqrt{3}}\right), \left(\frac{1}{\sqrt{3}}, -\frac{1}{\sqrt{3}}\right), \left(\frac{1}{\sqrt{3}}, \frac{1}{\sqrt{3}}\right)\right]$. The full diagram with all surface forces (which are 14 in number) with the coefficients of $\boldsymbol{\omega}^h$ are shown in Figure 3.4.

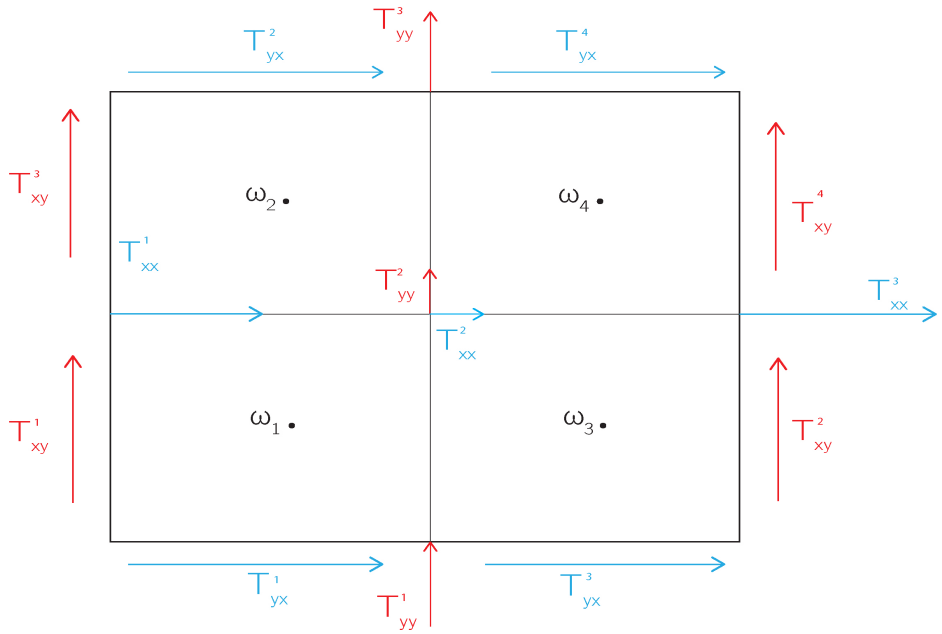

Figure 3.4: Complete single element

3.3.2 Setup

Now that we have what is required, we set up the scheme. We begin by working with the complementary energy functional where we substitute the expansions for stress,

$$\frac{1}{2}\int_{-1}^{1}\int_{-1}^{1}\boldsymbol{\sigma}^T C\boldsymbol{\sigma}\ \mathrm{d}x\mathrm{d}y = \frac{1}{30E}\left[2\left(T_{xx}^1\right)^2+8\left(T_{xx}^2\right)^2+2\left(T_{xx}^3\right)^2+2T_{xx}^1T_{xx}^2-T_{xx}^1T_{xx}^3\right.$$
$$\left.+2T_{xx}^2T_{xx}^3\right]$$
$$+\frac{1}{30E}\left[2\left(T_{yy}^1\right)^2+8\left(T_{yy}^2\right)^2+2\left(T_{yy}^3\right)^2+2T_{yy}^1T_{yy}^2-T_{yy}^1T_{yy}^3\right.$$
$$\left.+2T_{yy}^2T_{yy}^3\right]$$
$$+\frac{7(1+\nu)}{18E}\left[\left(T_{xy}^1\right)^2+\left(T_{xy}^2\right)^2+\left(T_{xy}^3\right)^2+\left(T_{xy}^4\right)^2+\left(T_{yx}^1\right)^2\right.$$
$$+\left(T_{yx}^2\right)^2+\left(T_{yx}^3\right)^2+\left(T_{yx}^4\right)^2+T_{xy}^1T_{xy}^2+T_{yx}^1T_{yx}^2+T_{xy}^3T_{xy}^4$$
$$\left.+T_{yx}^3T_{yx}^4\right]$$
$$-\frac{(1+\nu)}{18E}\left[2T_{xy}^1T_{xy}^3+2T_{yx}^1T_{yx}^3+2T_{xy}^2T_{xy}^4+2T_{yx}^2T_{yx}^4+T_{xy}^1T_{xy}^4\right.$$
$$\left.+T_{yx}^1T_{yx}^4+T_{xy}^2T_{xy}^3+T_{yx}^2T_{yx}^3\right]$$
$$-\frac{\nu}{36E}\left[T_{xx}^1T_{yy}^1+4T_{xx}^1T_{yy}^2+T_{xx}^1T_{yy}^3+4T_{xx}^2T_{yy}^1+16T_{xx}^2T_{yy}^2\right.$$
$$\left.+4T_{xx}^2T_{yy}^3+T_{xx}^3T_{yy}^1+4T_{xx}^3T_{yy}^2+T_{xx}^3T_{yy}^3\right],$$

where C is used from equation (3.12). It can be seen that the result is obtained in terms of all the surface forces present in the element. Taking variations with respect to each of the forces form a row in the mass matrix $\mathcal{M}$. Since there are 14 forces, the matrix will contain 14 rows and 14 columns. The RHS vector will contain zeros with respect to each of these rows. The matrix is also found to be symmetric as will be discussed later when we attempt to extend the scheme to multiple elements.

We now work with the constraints imposing conservation of linear momentum,

$$\int_{-1}^{1}\int_{-1}^{1}u^h\left\{\frac{\partial\sigma_{xx}^h}{\partial x}+\frac{\partial\sigma_{yx}^h}{\partial y}\right\}\mathrm{d}x\mathrm{d}y =$$
$$\left(\frac{1}{2}+\frac{1}{3}\sqrt{3}\right)u^1\left[T_{xx}^2-T_{xx}^1+T_{yx}^2-T_{yx}^1\right]+\left(\frac{1}{2}-\frac{1}{3}\sqrt{3}\right)u^2\left[T_{xx}^2-T_{xx}^1+T_{yx}^2-T_{yx}^1\right]+$$
$$\left(\frac{1}{2}-\frac{1}{3}\sqrt{3}\right)u^1\left[T_{xx}^3-T_{xx}^2+T_{yx}^4-T_{yx}^3\right]+\left(\frac{1}{2}+\frac{1}{3}\sqrt{3}\right)u^2\left[T_{xx}^3-T_{xx}^2+T_{yx}^4-T_{yx}^3\right],$$

$$\int_{-1}^{1}\int_{-1}^{1}v^h\left\{\frac{\partial\sigma_{xy}^h}{\partial x}+\frac{\partial\sigma_{yy}^h}{\partial y}\right\}\mathrm{d}x\mathrm{d}y =$$
$$\left(\frac{1}{2}+\frac{1}{3}\sqrt{3}\right)v^1\left[T_{xy}^2-T_{xy}^1+T_{yy}^2-T_{yy}^1\right]+\left(\frac{1}{2}-\frac{1}{3}\sqrt{3}\right)v^2\left[T_{xy}^2-T_{xy}^1+T_{yy}^2-T_{yy}^1\right]+$$
$$\left(\frac{1}{2}-\frac{1}{3}\sqrt{3}\right)v^1\left[T_{xy}^4-T_{xy}^3+T_{yy}^3-T_{yy}^2\right]+\left(\frac{1}{2}+\frac{1}{3}\sqrt{3}\right)v^2\left[T_{xy}^4-T_{xy}^3+T_{yy}^3-T_{yy}^2\right].$$

This time, we take variations with respect to u^1,u^2,v^1 and v^2 and continue building the matrix on the original matrix. This new matrix will be called $\mathcal{CL}$ is placed below the mass matrix $\mathcal{M}$. Then, variations are taken with respect to each of the other terms (forces) and the corresponding columns are added. This is equivalent to adding the transpose of the $\mathcal{CL}$. Finally, imposing symmetry of stress tensor (a consequence of conservation of angular momentum),

$$\int_{-1}^{1}\int_{-1}^{1} \omega^h \left[\sigma^h_{yx} - \sigma^h_{xy}\right] \mathrm{d}x\mathrm{d}y \ ,$$

we will again have terms involving the surface forces and coefficients ω^1, ω^2, ω^3 and ω^4. We take variations with respect to each of these coefficients and build the matrix $\mathcal{CA}$ below $\mathcal{M}$ and $\mathcal{CL}$. Similarly, variations are taken with respect to the other terms and the corresponding columns are added to the matrix. This is equivalent to adding the transpose of the $\mathcal{CA}$ matrix. Both $\mathcal{CL}$ and $\mathcal{CA}$ are not square matrices; each of them correspond to a size of 4×14. The system to be solved is,

$$\begin{pmatrix} \mathcal{M} & \mathcal{CL}^T & \mathcal{CA}^T \\ \mathcal{CL} & 0 & 0 \\ \mathcal{CA} & 0 & 0 \end{pmatrix} \begin{bmatrix} \mathscr{T} \\ \mathscr{U} \\ \mathscr{W} \end{bmatrix} = \begin{bmatrix} 0 \\ 0 \\ 0 \end{bmatrix} \ , \tag{3.26}$$

where the square form of the matrix has been retained. Also, $\mathscr{T}$, $\mathscr{U}$ and $\mathscr{W}$ are the vectors containing all the surface forces T^n_{ij} (where n represents the numbering), displacement coefficients u^i, v^i and rotation coefficients ω^i respectively. There are a total of **22 unknowns** to be determined. The matrix on the Left Hand Side (LHS) is the Global matrix $\mathcal{G}$ and it is **non-singular**, meaning that it will produce a **unique solution**. Note that this system at the moment does not contain any prescribed displacements, loads or even body forces; it is just a homogeneous system of equations. Under these circumstances, the unique solution is,

$$\begin{bmatrix} \mathscr{T} \\ \mathscr{U} \\ \mathscr{W} \end{bmatrix} = \begin{bmatrix} 0 \\ 0 \\ 0 \end{bmatrix} \ , \tag{3.27}$$

which can also be written as,

$$\text{Ker}(\mathcal{G}) \;=\; 0, \tag{3.28}$$

where the Kernel of a real matrix M of order $p \times q$ is defined as, [5],

$$\text{Ker}(M) \;:=\; \{x \in \mathbb{R}^p, \text{such that } Mx = 0_q\}\,.$$

3.3.3 Test cases

In the introduction of hybrid formulations, it was discussed that most hybrid schemes generate non-physical solutions that are attributed to Spurious Kinematic Modes (SKMs) that are independent of mesh size. To see if the scheme is free from such modes, we have to perform simple test cases before extending the scheme to multiple elements and applying hybrid ideas at their interfaces. The test case to be discussed are simple translations and rotations for which we must invoke the boundary integral which is part of the complementary energy functional in equation (3.11),

$$-\int_{\Gamma_u} \boldsymbol{t}^T \bar{\boldsymbol{u}}\, \mathrm{d}\Gamma \;= -\int_{\Gamma_u} \left[\sigma_{xx} n_x + \sigma_{yx} n_y\right] \bar{u}\;\, d\Gamma - \int_{\Gamma_u} \left[\sigma_{xy} n_x + \sigma_{yy} n_y\right] \bar{v}\;\, d\Gamma, \tag{3.29}$$

where we have prescribed displacements $\bar{\boldsymbol{u}} = [\bar{u},\ \bar{v}]^T$ over the entire boundary and have dropped the superscript h for the sake of convenience. We first work with the X configuration in Figure 3.2 and then move to the Y configuration in Figure 3.3.

Working with the left boundary, we have $n_x = -1, n_y = 0$ and $\sigma_{xx}\Big|_{x=-1} = \frac{1}{2}\, T^1_{xx}$. We get,

$$\int_{-1}^{1} \frac{T^1_{xx}}{2}\, \bar{u}\, \mathrm{d}y \;=\; T^1_{xx}\, \bar{u}\,.$$

We take the derivative of T^1_{xx} and are left with $\bar{u}$ which we move to the first row of RHS vector in equation (3.26) to become $-\bar{u}$. This way, we have prescribed a displacement on the left boundary with respect to normal stress σ_{xx}. With the same boundary, we also have the shear stress σ_{xy}. We have $n_x = -1, n_y = 0$ and,

$$\sigma_{xy}\Big|_{x=-1} = \frac{1}{2}(1-2y)\,T^1_{xy} \;+\; \frac{1}{2}(1+2y)\,T^3_{xy}$$

We get,

$$\int_{-1}^{1}\left[\frac{1}{2}(1-2y)\,T^1_{xy} \;+\; \frac{1}{2}(1+2y)\,T^3_{xy}\right]\bar{v}\;\mathrm{d}y \;=\; \left(T^1_{xy} \;+T^3_{xy}\right)\bar{v}\;.$$

Taking variations with respect to T^1_{xy} and T^3_{xy} separately, will yield a displacement of $\bar{v}$ which is moved to the RHS to give $-\bar{v}$. Following the same procedure for all boundaries, the RHS vector becomes,

$$\mathcal{R} \;=\; [-\bar{u},\;0,\;\bar{u},-\bar{u},\;\bar{u},-\bar{u},\;\bar{u},-\bar{v},\;0,\;\bar{v},-\bar{v},\;\bar{v},-\bar{v},\;\bar{v}]^T,$$

where the zero's correspond to rows where the variations were taken with respect to internal forces T^2_{xx} and T^2_{yy}. If we now prescribe a displacement of $\bar{u}=2$ and $\bar{v}=3$, we are translating the body 2 units in the X direction and 3 units in the Y direction. Realistically, in the absence of loading and assuming linear and angular equilibrium, the body must not experience any stresses. Firstly, the code shows that the $\mathcal{G}$ matrix is non-singular. The solution vector shows that all surface forces and ω^i's have a value of zero (upto machine precision) while $u^i=2$ and $v_i=3$. Since the surface forces are zero, the stresses are zero. There are no SKMs either so we have the perfect result for translations.

If we want to impose a rotation of magnitude $\bar{\omega}$, it can be done by setting $\bar{u}=-\bar{\omega}y$ and $\bar{v}=\bar{\omega}x$. We will work with the top boundary this time and once again work with the X configuration first. We have $n_x=0$ and $n_y=1$. The integral is,

$$-\int_{-1}^{1}\sigma_{yx}|_{y=1}\;(-\bar{\omega}\cdot 1)\;\mathrm{d}x \;=\; \bar{\omega}\left(T^2_{yx}+T^4_{yx}\right)\;.$$

Taking variations with respect to T^2_{yx} and T^4_{yx} separately, will yield a rotation of $\bar{\omega}$ which is moved to the RHS to give $-\bar{\omega}$. For the same boundary, we also have the normal stress σ_{yy}. The integral is,

$$-\int_{-1}^{1}\sigma_{yy}|_{y=1}\;(\bar{\omega}x)\;\mathrm{d}x \;=\; -\frac{T^3_{yy}\,\bar{\omega}}{2}\left(\frac{x^2}{2}\right)\Bigg|_{-1}^{1}=0\;,$$

an important result for the single element. Normal forces do not cause rotation of the element in the single element case. Following the same procedure for all boundaries, the RHS vector becomes,

$$\mathcal{W} \;=\; [0,\ 0,\ 0,\ 0,\ \bar{\omega},\ \bar{\omega},\ \bar{\omega},\ \bar{\omega},\ 0,\ 0,\ 0,\ 0, -\bar{\omega}, -\bar{\omega}, -\bar{\omega}, -\bar{\omega}]^T.$$

Again, we expect no stresses to be generated since the body is not deformed in any way and neither have we applied external loading or internal body forces. If we now prescribe a rotation of magnitude $\bar{\omega} = 10$ and solve the system, we see that $\mathcal{G}$ is non-singular and hence permits a unique solution. We find that all the surface forces (and hence stresses) and displacements u^i, v^i are equal to zero (upto machine precision) while the $\omega^i = 10$. The result is again, perfect. No SKM's were found.

3.3.4 Physical domain

Now that we have performed a basic test case, we can move on to build a scheme for multiple elements and then applying hybrid ideas. To do this, we must transform from $\Omega = [-1\ \ 1]^2$ to a new orthogonal domain $\Omega = [0\ \ h_1] \times [0\ \ h_2]$ so that we can work with smaller elements. The finite dimensional representations for stress now become,

$$\sigma_{xx}(x,y) \;=\; T^1_{xx}\frac{2}{h_2(h_1)^2}\left(x-\frac{h_1}{2}\right)(x-h_1) \;-\; T^2_{xx}\frac{4}{h_2(h_1)^2}x\,(x-h_1) \;+\; T^3_{xx}\frac{2}{h_2(h_1)^2}x\left(x-\frac{h_1}{2}\right), \tag{3.30}$$

$$\begin{aligned}\sigma_{yx}(x,y) \;=\; & T^1_{yx}\frac{4}{h_2(h_1)^2}\left(\frac{3h_1}{4}-x\right)(h_2-y) \;+\; T^2_{yx}\frac{4}{h_2(h_1)^2}\left(\frac{3h_1}{4}-x\right)y \;+ \\ & T^3_{yx}\frac{4}{h_2(h_1)^2}\left(x-\frac{h_1}{4}\right)(h_2-y) \;+\; T^4_{yx}\frac{4}{h_2(h_1)^2}\left(x-\frac{h_1}{4}\right)y\,,\end{aligned} \tag{3.31}$$

$$\sigma_{yy}(x,y) \;=\; T^1_{yy}\frac{2}{h_1(h_2)^2}\left(y-\frac{h_2}{2}\right)(y-h_2) \;-\; T^2_{yy}\frac{4}{h_1(h_2)^2}y\,(y-h_2) \;+\; T^3_{yy}\frac{2}{h_1(h_2)^2}y\left(y-\frac{h_2}{2}\right),$$

$$\begin{aligned}\sigma_{xy}(x,y) \;=\; & T^1_{xy}\frac{4}{h_1(h_2)^2}\left(\frac{3h_2}{4}-y\right)(h_1-x) \;+\; T^2_{xy}\frac{4}{h_1(h_2)^2}\left(\frac{3h_2}{4}-y\right)x \;+ \\ & T^3_{xy}\frac{4}{h_1(h_2)^2}\left(y-\frac{h_2}{4}\right)(h_1-x) \;+\; T^4_{xy}\frac{4}{h_1(h_2)^2}\left(y-\frac{h_2}{4}\right)x\,.\end{aligned}$$

If we use coordinates ξ and η for the first (computational) domain $[-1\ \ 1]^2$, we can use the following transformation to get to the new domain $[0\ \ h_1] \times [0\ \ h_2]$,

$$\xi \ = \ \frac{2x}{h_1} - 1, \qquad \eta \ = \ \frac{2y}{h_2} - 1, \tag{3.32}$$

so that,

$$\int_0^{h_2} \int_0^{h_1} \mathrm{d}x\mathrm{d}y \ = \ \frac{1}{4} \int_{-1}^{1} \int_{-1}^{1} h_1 h_2 \mathrm{d}\xi\mathrm{d}\eta.$$

Note that, for $h_1 = h_2 = 2$, $[-1\ \ 1]^2 \equiv [0\ \ 2]^2$. The complementary energy is given by,

$$\frac{1}{2} \int_0^{h_2} \int_0^{h_1} \sigma^T(x,y) C \sigma(x,y) \ \mathrm{d}x\mathrm{d}y \ = \ \frac{1}{8} \int_{-1}^{1} \int_{-1}^{1} \sigma^T(\xi,\eta) C \sigma(\xi,\eta) \ h_1 h_2 \mathrm{d}\xi\mathrm{d}\eta,$$

which is different from the one element case given by,

$$\frac{1}{2} \int_{-1}^{1} \int_{-1}^{1} \sigma^T C \sigma \ \mathrm{d}\xi\mathrm{d}\eta$$

where the computational and physical domain were exactly the same ($x = \xi$ and $y = \eta$). This indicates that the mass matrix will definitely change. The original $\mathcal{M}$ is given by,

$$\mathcal{M} = \begin{pmatrix}
\frac{2}{15E} & \frac{1}{15E} & \frac{-1}{30E} & 0 & 0 & 0 & 0 & \frac{-\nu}{36E} & \frac{-\nu}{9E} & \frac{-\nu}{36E} & 0 & 0 & 0 & 0 \\
\frac{1}{15E} & \frac{8}{15E} & \frac{1}{15E} & 0 & 0 & 0 & 0 & \frac{-\nu}{9E} & \frac{-4\nu}{9E} & \frac{-\nu}{9E} & 0 & 0 & 0 & 0 \\
\frac{-1}{30E} & \frac{1}{15E} & \frac{2}{15E} & 0 & 0 & 0 & 0 & \frac{-\nu}{36E} & \frac{-\nu}{9E} & \frac{-\nu}{36E} & 0 & 0 & 0 & 0 \\
0 & 0 & 0 & \frac{7(1+\nu)}{9E} & \frac{7(1+\nu)}{18E} & \frac{-(1+\nu)}{9E} & \frac{-(1+\nu)}{18E} & 0 & 0 & 0 & 0 & 0 & 0 & 0 \\
0 & 0 & 0 & \frac{7(1+\nu)}{18E} & \frac{7(1+\nu)}{9E} & \frac{-(1+\nu)}{18E} & \frac{-(1+\nu)}{9E} & 0 & 0 & 0 & 0 & 0 & 0 & 0 \\
0 & 0 & 0 & \frac{-(1+\nu)}{9E} & \frac{-(1+\nu)}{18E} & \frac{7(1+\nu)}{9E} & \frac{7(1+\nu)}{18E} & 0 & 0 & 0 & 0 & 0 & 0 & 0 \\
0 & 0 & 0 & \frac{-(1+\nu)}{18E} & \frac{-(1+\nu)}{9E} & \frac{7(1+\nu)}{18E} & \frac{7(1+\nu)}{9E} & 0 & 0 & 0 & 0 & 0 & 0 & 0 \\
\frac{-\nu}{36E} & \frac{-\nu}{9E} & \frac{-\nu}{36E} & 0 & 0 & 0 & 0 & \frac{2}{15E} & \frac{1}{15E} & \frac{-1}{30E} & 0 & 0 & 0 & 0 \\
\frac{-\nu}{9E} & \frac{-4\nu}{9E} & \frac{-\nu}{9E} & 0 & 0 & 0 & 0 & \frac{1}{15E} & \frac{8}{15E} & \frac{1}{15E} & 0 & 0 & 0 & 0 \\
\frac{-\nu}{36E} & \frac{-\nu}{9E} & \frac{-\nu}{36E} & 0 & 0 & 0 & 0 & \frac{-1}{30E} & \frac{1}{15E} & \frac{2}{15E} & 0 & 0 & 0 & 0 \\
0 & 0 & 0 & 0 & 0 & 0 & 0 & 0 & 0 & 0 & \frac{7(1+\nu)}{9E} & \frac{7(1+\nu)}{18E} & \frac{-(1+\nu)}{9E} & \frac{-(1+\nu)}{18E} \\
0 & 0 & 0 & 0 & 0 & 0 & 0 & 0 & 0 & 0 & \frac{7(1+\nu)}{18E} & \frac{7(1+\nu)}{9E} & \frac{-(1+\nu)}{18E} & \frac{-(1+\nu)}{9E} \\
0 & 0 & 0 & 0 & 0 & 0 & 0 & 0 & 0 & 0 & \frac{-(1+\nu)}{9E} & \frac{-(1+\nu)}{18E} & \frac{7(1+\nu)}{9E} & \frac{7(1+\nu)}{18E} \\
0 & 0 & 0 & 0 & 0 & 0 & 0 & 0 & 0 & 0 & \frac{-(1+\nu)}{18E} & \frac{-(1+\nu)}{9E} & \frac{7(1+\nu)}{18E} & \frac{7(1+\nu)}{9E}
\end{pmatrix}$$

The new Mass matrix $\mathcal{M}_h$ is given by,

$$\begin{pmatrix}
\frac{2}{15E}\frac{h_1}{h_2} & \frac{1}{15E}\frac{h_1}{h_2} & \frac{-1}{30E}\frac{h_1}{h_2} & 0 & 0 & 0 & 0 & \frac{-\nu}{36E} & \frac{-\nu}{9E} & \frac{-\nu}{36E} & 0 & 0 & 0 & 0 \\
\frac{1}{15E}\frac{h_1}{h_2} & \frac{8}{15E}\frac{h_1}{h_2} & \frac{1}{15E}\frac{h_1}{h_2} & 0 & 0 & 0 & 0 & \frac{-\nu}{9E} & \frac{-4\nu}{9E} & \frac{-\nu}{9E} & 0 & 0 & 0 & 0 \\
\frac{-1}{30E}\frac{h_1}{h_2} & \frac{1}{15E}\frac{h_1}{h_2} & \frac{2}{15E}\frac{h_1}{h_2} & 0 & 0 & 0 & 0 & \frac{-\nu}{36E} & \frac{-\nu}{9E} & \frac{-\nu}{36E} & 0 & 0 & 0 & 0 \\
0 & 0 & 0 & \frac{7(1+\nu)}{9E}\frac{h_2}{h_1} & \frac{7(1+\nu)}{18E}\frac{h_2}{h_1} & \frac{-(1+\nu)}{9E}\frac{h_2}{h_1} & \frac{-(1+\nu)}{18E}\frac{h_2}{h_1} & 0 & 0 & 0 & 0 & 0 & 0 & 0 \\
0 & 0 & 0 & \frac{7(1+\nu)}{18E}\frac{h_2}{h_1} & \frac{7(1+\nu)}{9E}\frac{h_2}{h_1} & \frac{-(1+\nu)}{18E}\frac{h_2}{h_1} & \frac{-(1+\nu)}{9E}\frac{h_2}{h_1} & 0 & 0 & 0 & 0 & 0 & 0 & 0 \\
0 & 0 & 0 & \frac{-(1+\nu)}{9E}\frac{h_2}{h_1} & \frac{-(1+\nu)}{18E}\frac{h_2}{h_1} & \frac{7(1+\nu)}{9E}\frac{h_2}{h_1} & \frac{7(1+\nu)}{18E}\frac{h_2}{h_1} & 0 & 0 & 0 & 0 & 0 & 0 & 0 \\
0 & 0 & 0 & \frac{-(1+\nu)}{18E}\frac{h_2}{h_1} & \frac{-(1+\nu)}{9E}\frac{h_2}{h_1} & \frac{7(1+\nu)}{18E}\frac{h_2}{h_1} & \frac{7(1+\nu)}{9E}\frac{h_2}{h_1} & 0 & 0 & 0 & 0 & 0 & 0 & 0 \\
\frac{-\nu}{36E} & \frac{-\nu}{9E} & \frac{-\nu}{36E} & 0 & 0 & 0 & 0 & \frac{2}{15E}\frac{h_2}{h_1} & \frac{1}{15E}\frac{h_2}{h_1} & \frac{-1}{30E}\frac{h_2}{h_1} & 0 & 0 & 0 & 0 \\
\frac{-\nu}{9E} & \frac{-4\nu}{9E} & \frac{-\nu}{9E} & 0 & 0 & 0 & 0 & \frac{1}{15E}\frac{h_2}{h_1} & \frac{8}{15E}\frac{h_2}{h_1} & \frac{1}{15E}\frac{h_2}{h_1} & 0 & 0 & 0 & 0 \\
\frac{-\nu}{36E} & \frac{-\nu}{9E} & \frac{-\nu}{36E} & 0 & 0 & 0 & 0 & \frac{-1}{30E}\frac{h_2}{h_1} & \frac{1}{15E}\frac{h_2}{h_1} & \frac{2}{15E}\frac{h_2}{h_1} & 0 & 0 & 0 & 0 \\
0 & 0 & 0 & 0 & 0 & 0 & 0 & 0 & 0 & 0 & \frac{7(1+\nu)}{9E}\frac{h_1}{h_2} & \frac{7(1+\nu)}{18E}\frac{h_1}{h_2} & \frac{-(1+\nu)}{9E}\frac{h_1}{h_2} & \frac{-(1+\nu)}{18E}\frac{h_1}{h_2} \\
0 & 0 & 0 & 0 & 0 & 0 & 0 & 0 & 0 & 0 & \frac{7(1+\nu)}{18E}\frac{h_1}{h_2} & \frac{7(1+\nu)}{9E}\frac{h_1}{h_2} & \frac{-(1+\nu)}{18E}\frac{h_1}{h_2} & \frac{-(1+\nu)}{9E}\frac{h_1}{h_2} \\
0 & 0 & 0 & 0 & 0 & 0 & 0 & 0 & 0 & 0 & \frac{-(1+\nu)}{9E}\frac{h_1}{h_2} & \frac{-(1+\nu)}{18E}\frac{h_1}{h_2} & \frac{7(1+\nu)}{9E}\frac{h_1}{h_2} & \frac{7(1+\nu)}{18E}\frac{h_1}{h_2} \\
0 & 0 & 0 & 0 & 0 & 0 & 0 & 0 & 0 & 0 & \frac{-(1+\nu)}{18E}\frac{h_1}{h_2} & \frac{-(1+\nu)}{9E}\frac{h_1}{h_2} & \frac{7(1+\nu)}{18E}\frac{h_1}{h_2} & \frac{7(1+\nu)}{9E}\frac{h_1}{h_2}
\end{pmatrix}$$

where the dependence on element size is clearly seen. Therefore, changing the mesh size changes the values of the Mass matrix. To be clear, the (three) diagonals are seen to be dependent on mesh size ratio while the off-diagonal elements are independent of this ratio. For $h_1 = h_2$, the two matrices match exactly. Similarly, even basis functions $u^h, v^h, \boldsymbol{\omega}^h$ change due to this new domain. The basis function $u^h(x, y)$ for $[0\ \ h_1]$ is,

$$u^h(x,y) = u^1 \frac{1}{2}\left(1 + \sqrt{3} - \frac{2\sqrt{3}x}{h_1}\right) + u^2 \frac{1}{2}\left(1 - \sqrt{3} + \frac{2\sqrt{3}x}{h_1}\right).$$

Similarly, the basis function $v^h(x, y)$ for $[0\ \ h_2]$ is,

$$v^h(x,y) = v^1 \frac{1}{2}\left(1 + \sqrt{3} - \frac{2\sqrt{3}y}{h_2}\right) + v^2 \frac{1}{2}\left(1 - \sqrt{3} + \frac{2\sqrt{3}y}{h_2}\right).$$

These Lagrange multipliers enforce the linear momentum constraint in X and Y directions respectively in the following way,

$$\int_0^{h_2}\int_0^{h_1} u^h \left\{\frac{\partial \sigma^h_{xx}}{\partial x} + \frac{\partial \sigma^h_{yx}}{\partial y}\right\} \mathrm{d}x\mathrm{d}y\ ,$$
$$\int_0^{h_2}\int_0^{h_1} v^h \left\{\frac{\partial \sigma^h_{xy}}{\partial x} + \frac{\partial \sigma^h_{yy}}{\partial y}\right\} \mathrm{d}x\mathrm{d}y\ .$$

Computing the linear momentum matrix $\mathcal{CL}$ shows independence of mesh size ratio. Hence, the result is the same as it was for the single element case; that is, $\mathcal{CL}$ remains unchanged. We must now compute the angular momentum matrix to see if it is independent of mesh size as well. The basis function for rotation becomes,

$$\begin{aligned}\boldsymbol{\omega}^h(x,y) \;=\; & \omega^1\frac{1}{4}\left(1+\sqrt{3}-\frac{2\sqrt{3}x}{h_1}\right)\left(1+\sqrt{3}-\frac{2\sqrt{3}y}{h_2}\right) \;+\; \omega^2\frac{1}{4}\left(1+\sqrt{3}-\frac{2\sqrt{3}x}{h_1}\right) \\ & \left(1-\sqrt{3}+\frac{2\sqrt{3}y}{h_2}\right) \;+\omega^3\frac{1}{4}\left(1-\sqrt{3}+\frac{2\sqrt{3}x}{h_1}\right)\left(1+\sqrt{3}-\frac{2\sqrt{3}y}{h_2}\right) \;+\; \omega^4\frac{1}{4} \\ & \left(1-\sqrt{3}+\frac{2\sqrt{3}x}{h_1}\right)\left(1-\sqrt{3}+\frac{2\sqrt{3}y}{h_2}\right) .\end{aligned}$$

The rotation function is used as a Lagrange multiplier to enforce symmetry of stress tensor in the following way,

$$\int_0^{h_2}\int_0^{h_1} \boldsymbol{\omega}^h\left[\sigma^h_{yx}-\sigma^h_{xy}\right]\mathrm{d}x\mathrm{d}y \; .$$

Later, it will be shown that the rotation field indeed imposes symmetry of stress successfully. However something goes wrong with the rotation field $\boldsymbol{\omega}^h$ itself as it is found to be discontinuous and diverges from the exact solution as shown in Figures 4.18, 4.19 and 4.21.

3.4 Multiple elements

It is now known how a single element can be set up. What about multiple elements? Where do we place them and how do they work? What could make a compatible hybrid formulation? The answers to these questions are attempted here, step by step. Recall the matrix system for one element, which is rewritten here with no prescribed displacements and body forces,

$$\begin{pmatrix}\mathcal{M} & \mathcal{CL}^T & \mathcal{CA}^T \\ \mathcal{CL} & 0 & 0 \\ \mathcal{CA} & 0 & 0\end{pmatrix}\begin{bmatrix}\mathscr{T} \\ \mathscr{U} \\ \mathscr{W}\end{bmatrix} \;=\; \begin{bmatrix}0 \\ 0 \\ 0\end{bmatrix} \; . \tag{3.33}$$

where we denote the LHS matrix of element i by $\mathcal{G}_i$,

$$\mathcal{G}_i \;=\; \begin{pmatrix} \mathcal{M} & \mathcal{C}\mathcal{L}^T & \mathcal{C}\mathcal{A}^T \\ \mathcal{C}\mathcal{L} & 0 & 0 \\ \mathcal{C}\mathcal{A} & 0 & 0 \end{pmatrix} .$$

To get an idea of multiple elements, take a look at Figure 3.5. These elements are basically packed inside the physical domain, say $[-1 \;\; 1]^2$. In the numerical scheme, we arrange each of the elements in a diagonal matrix in the following way,

$$\begin{pmatrix} \mathcal{G}_1 & & & & & & \\ & \mathcal{G}_2 & & & & & \\ & & \ddots & & & & \\ & & & \mathcal{G}_i & & & \\ & & & & \ddots & & \\ & & & & & \mathcal{G}_n & \end{pmatrix} . \tag{3.34}$$

The system to be solved then becomes,

$$\begin{pmatrix} \mathcal{G}_1 & & & & & & \\ & \mathcal{G}_2 & & & & & \\ & & \ddots & & & & \\ & & & \mathcal{G}_i & & & \\ & & & & \ddots & & \\ & & & & & \mathcal{G}_n & \end{pmatrix} \begin{bmatrix} \mathcal{S}_1 \\ \mathcal{S}_2 \\ \vdots \\ \mathcal{S}_i \\ \vdots \\ \mathcal{S}_n \end{bmatrix} \;=\; \begin{bmatrix} 0 \\ \vdots \\ \vdots \\ \vdots \\ \vdots \\ 0 \end{bmatrix} . \tag{3.35}$$

where $\mathcal{S}_i$ contains the 22 unknowns of element i. That is,

$$\mathcal{S}_i \;=\; [\mathscr{T}_i \;\; \mathscr{U}_i \;\; \mathscr{W}_i]^T .$$

While a unique solution could exist for equation (3.35), there will be discontinuous jumps of forces (and hence, stresses) from one element to another. This, obviously

is incorrect. To rectify this, we have to impose continuity of the stresses between the elements that are in contact with eachother. This is also known as applying the interface displacements or 'glue' between the elements. In order to apply these hybrid ideas, we use Lagrange multipliers yet again; which brings us to the next subsection.

3.4.1 Interface potential

Once again, we want to present two separate figures; one which shows all the Lagrange multipliers involved in coupling *internal* forces involved in the X direction (Figure 3.5) and another which shows the Lagrange multipliers involved in coupling internal forces forces involved in the Y direction (Figure 3.6). Here, the elements have been labelled with the aid of Roman numerals. In the X direction, the internal forces involved are the normal forces: T^1_{xx} and T^3_{xx} and the shear force pairs T^1_{yx}, T^3_{yx} and T^2_{yx}, T^4_{yx}. You can have a look at Figure 3.2 for the convention for the forces.

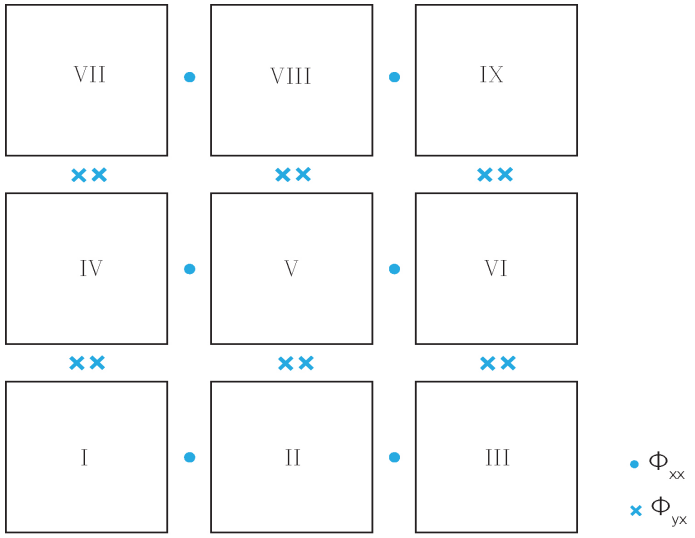

Figure 3.5: Multiple elements, X-configuration

Note that each of the cells (elements) in the Figures are of size $[0\ h_1] \times [0\ h_2]$. To see how we can impose the interface potential, consider imposing continuity between elements IV and V. Since there is only one dof between these elements, the Lagrange multiplier is a constant function; that is $\phi_{xx}(y) = \phi_{xx}$ that works in the following way,

$$\int_0^{h_2} \phi_{xx} \left(\sigma^{IV}_{xx}(x = h_1) - \sigma^{V}_{xx}(x = 0) \right) \, \mathrm{d}y \;=\; 0 \qquad \forall \phi_{xx}, \tag{3.36}$$

$$\int_0^{h_2} \phi_{xx} \left(\frac{1}{h_2} T_{xx}^{3,IV} - \frac{1}{h_2} T_{xx}^{1,V} \right) \, \mathrm{d}y \;=\; 0 \,,$$

or,

$$\phi_{xx} \left(T_{xx}^{3,IV} - T_{xx}^{1,V} \right) \;=\; 0 \,. \tag{3.37}$$

where the expansion in equation (3.30) has been used. Recall that we want to add these ideas to our scheme. In order to add this, we have to take variations with respect to ϕ_{xx} and equate them to zero, leading to,

$$T_{xx}^{3,IV} - T_{xx}^{1,V} \;=\; 0 \,.$$

This result is added as a new row in our system (3.35) and its transpose is added as a column after taking variations with respect to $T_{xx}^{3,IV}$ and $T_{xx}^{1,V}$. As a consequence, the matrix retains its square form. Similarly, this is extended to all elements in the figure to connect the normal forces T_{xx}^{1} and T_{xx}^{3}.

For coupling shear forces, we can't use just one Lagrange multiplier since there are 4 forces involved at the interface between elements. If we want to impose continuity in between element I and IV (for example), we should use a linear basis function (expanded in terms of Gauss points) for the Lagrange multiplier ϕ_{yx} that is linear in X and constant in Y due to two degrees of freedom in the X direction. Also, noting that the coordinates are $[0 \;\; h_1] \times [0 \;\; h_2]$, we can use the transformed basis function, again expanded in terms of the Gauss points relevant to this interval,

$$\phi_{yx}(x,y) = \phi^1 \frac{1}{2} \left(1 + \sqrt{3} - \frac{2\sqrt{3}x}{h_1} \right) + \phi^2 \frac{1}{2} \left(1 - \sqrt{3} + \frac{2\sqrt{3}x}{h_1} \right) \,.$$

Now, we impose the continuity for shear stress between Elements I and IV ,

$$\int_0^{h_1} \phi_{yx}(x,y) \left[\sigma_{yx}^{I}(y = h_2) - \sigma_{yx}^{IV}(y = 0) \right] \;\; dx = 0 \qquad \forall \phi_{yx} \,, \tag{3.38}$$

which results in,

$$\phi^1_{yx}\frac{1}{\sqrt{3}}\left(-T^{1,IV}_{yx}+T^{2,I}_{yx}-T^{4,I}_{yx}+T^{3,IV}_{yx}\right) \;+\; \phi^1_{yx}\frac{1}{2}\left(-T^{1,IV}_{yx}+T^{2,I}_{yx}-T^{3,IV}_{yx}+T^{4,I}_{yx}\right)+$$
$$\phi^2_{yx}\frac{1}{\sqrt{3}}\left(T^{1,IV}_{yx}-T^{2,I}_{yx}+T^{4,I}_{yx}-T^{3,IV}_{yx}\right) \;+\; \phi^2_{yx}\frac{1}{2}\left(-T^{1,IV}_{yx}+T^{2,I}_{yx}-T^{3,IV}_{yx}+T^{4,I}_{yx}\right)=0 \quad \forall\phi_{yx}\;, \tag{3.39}$$

for which we must take variations with respect to ϕ^1_{yx} and ϕ^2_{yx} separately and equate them to zero,

$$\frac{1}{\sqrt{3}}\left(-T^{1,IV}_{yx}+T^{2,I}_{yx}-T^{4,I}_{yx}+T^{3,IV}_{yx}\right) \;+\; \frac{1}{2}\left(-T^{1,IV}_{yx}+T^{2,I}_{yx}-T^{3,IV}_{yx}+T^{4,I}_{yx}\right) \;=\; 0\;,$$

$$\frac{1}{\sqrt{3}}\left(T^{1,IV}_{yx}-T^{2,I}_{yx}+T^{4,I}_{yx}-T^{3,IV}_{yx}\right) \;+\; \frac{1}{2}\left(-T^{1,IV}_{yx}+T^{2,I}_{yx}-T^{3,IV}_{yx}+T^{4,I}_{yx}\right) \;=\; 0\;,$$

which are added as new rows in our system (3.35) and its transpose is added as a column (from taking variations with respect to the force terms). As a consequence, the square form of the matrix is retained once again. Similarly, this is extended to all elements in the figure to connect the shear force pairs T^1_{yx}, T^3_{yx} and T^2_{yx}, T^4_{yx}. Now that the procedure has been established, we repeat the same procedure with forces in the Y direction (Figure 3.6). Here, between elements I and IV we connect the normal forces T^1_{yy} and T^3_{yy} using,

$$\int_0^{h_1}\phi_{yy}\left(\sigma^I_{yy}(y=h_2)-\sigma^{IV}_{yy}(y=0)\right)\,\mathrm{d}x \;=\; 0 \quad \forall\phi_{yy}\;, \tag{3.40}$$

and the shear force pairs T^1_{xy}, T^3_{xy} and T^2_{xy}, T^4_{xy} between elements IV and V using,

$$\int_0^{h_2}\phi_{xy}(x,y)\left[\sigma^{IV}_{xy}(x=h_1)-\sigma^{V}_{xy}(x=0)\right]\,\mathrm{d}y=0 \quad \forall\phi_{xy}\;, \tag{3.41}$$

Equations (3.36), (3.38), (3.40) and (3.41), when combined for the interfaces of all elements, are added to the functional (in discrete form) in equation (3.13). By taking variations with respect to each of Lagrange multipliers, it is realised that they are indeed kinematic fields that impose linear and angular momentum equilibrium in the domain and continuity of forces between elements.

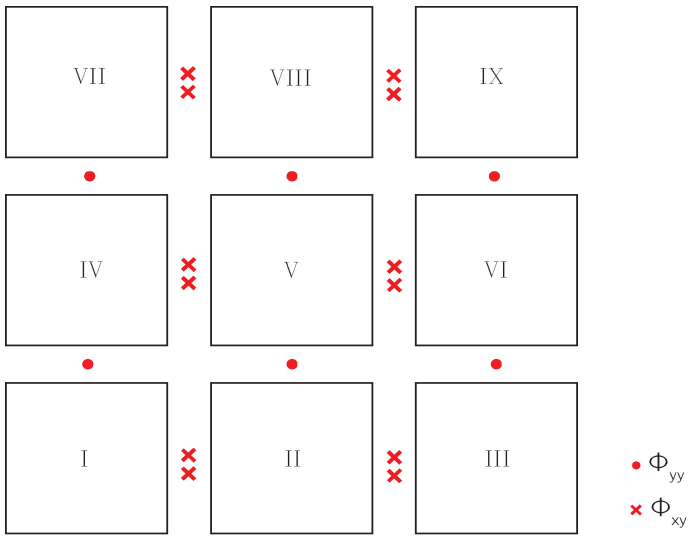

Figure 3.6: Multiple elements, Y-configuration

If we have K elements in the X direction and L elements in the Y direction, we will need $3(K-1)L+3K(L-1)$ Lagrange multipliers. For example, if we consider $K=L=2$, our new system for multiple elements, with the implementation of our hybrid ideas looks like this,

$$\begin{pmatrix} \mathcal{G}_1 & & & & \vdots & \mathcal{H}^T \\ & \mathcal{G}_2 & & & \vdots & \\ & & \mathcal{G}_3 & & \vdots & \\ & & & \mathcal{G}_4 & \vdots & \\ \cdots & \cdots & \cdots & \cdots & \cdot & \cdots \\ \mathcal{H} & & & & \vdots & 0 \end{pmatrix} \begin{bmatrix} \mathcal{S}_1 \\ \mathcal{S}_2 \\ \mathcal{S}_3 \\ \mathcal{S}_4 \\ \cdots \\ \Phi \end{bmatrix} = \begin{bmatrix} 0 \\ \vdots \\ \vdots \\ \vdots \\ \vdots \\ 0 \end{bmatrix}, \tag{3.42}$$

where Φ is a vector containing 12 Lagrange multipliers enforcing continuity between the internal forces of elements in contact and $\mathcal{H}$ matrix is known as the Hybrid matrix. Unfortunately, the matrix on the LHS was found to be singular in the kinematic modes (u^i, v^i, ω^i) as is generally the case. These are basically the Spurious Kinematic Modes (SKMs) that people working with hybrid formulations expect in their scheme. In the current scheme, for any K, L, the number of singularities are equivalent to $(K-1)(L-1)$; that is, the number of corner points where any 4 elements meet. For Figures 3.5 and 3.6, there are 4 such singularities corresponding to the 4 internal

corners. It was found that using just one Lagrange multiplier to couple four shear forces at the junction produces a non-singular system but post-processing results showed that the results were sub-optimal. Hence, the cause of this singular system can be attributed to having redundant Lagrange multipliers. One way to proceed from here is to solve the original singular system and check our results; we expect the stress fields to be physical because the singularities are always in the kinematic modes. Subsequently, we can try another technique to couple shear stresses with the hope for a non-singular system. The second way to go about it is to devise a way to remove the SKMs. [12], provides exhaustive literature on techniques to detect SKMs, how and under what conditions they can be removed from a scheme to make the matrix non-singular. The former method is preferred and used in this report; we proceed with the evaluation of the singular system in the next chapter for a specific test case.

Chapter 4

Test case

In order to validate our scheme, one of the ways is to manufacture a solution. We assume a specific displacement field over a sufficiently smooth domain Ω with a boundary $\Gamma(\Omega)$ after which, we compute strains. From this, we compute all the stresses using the compliance tensor.

We assume the components of the displacement field $\boldsymbol{u} = [u\ v]^T$,

$$u = \sin(2\pi x)\sin(2\pi y)\ , \qquad v = \sin(\pi x)\sin(\pi y)\ . \tag{4.1}$$

The components of strain are computed using equation (3.1),

$$\epsilon_{xx} = 2\pi \sin(2\pi y)\cos(2\pi x)\ , \quad \epsilon_{yy} = \pi \sin(\pi x)\cos(\pi y)\ ,$$

$$\epsilon_{yx} = \epsilon_{xy} = \pi \sin(2\pi x)\cos(2\pi y) + \frac{\pi}{2}\sin(\pi y)\cos(\pi x)\ .$$

Rotation ω_{xy} is calculated as,

$$\omega_{xy} \ = \ \frac{1}{2}\left[\pi \cos(\pi x)\sin(\pi y) - 2\pi \sin(2\pi x)\cos(2\pi y)\right]\ .$$

The stresses are computed using constitutive relations from Hooke's law of elasticity,

that is equation (3.3),

$$\sigma_{xx} = \frac{E}{1-\nu^2}\left(\epsilon_{xx} + \nu\epsilon_{yy}\right) \;=\; \frac{E}{1-\nu^2}\left[2\pi\sin(2\pi y)\cos(2\pi x) + \nu\pi\sin(\pi x)\cos(\pi y)\right] \;. \tag{4.2}$$

$$\sigma_{yy} = \frac{E}{1-\nu^2}\left(\epsilon_{yy} + \nu\epsilon_{xx}\right) \;=\; \frac{E}{1-\nu^2}\left[\pi\sin(\pi x)\cos(\pi y) + \nu\; 2\pi\sin(2\pi y)\cos(2\pi x)\right] \;. \tag{4.3}$$

$$\sigma_{yx} = \frac{E}{1+\nu}\epsilon_{yx} \;=\; \sigma_{xy} = \frac{E}{1+\nu}\epsilon_{xy} \;.$$

$$\sigma_{yx} = \sigma_{xy} = \frac{E}{1+\nu}\left[\pi\sin(2\pi x)\cos(2\pi y) + \frac{\pi}{2}\sin(\pi y)\cos(\pi x)\right] \;. \tag{4.4}$$

Conservation of linear momentum is given by,

$$\frac{\partial\sigma_{ij}}{\partial x_i} \;=\; -f_j \;, \tag{4.5}$$

In the X direction, using equations (4.2) and (4.4) we get,

$$\frac{\partial\sigma_{xx}}{\partial x} + \frac{\partial\sigma_{yx}}{\partial y} \;=\; -\frac{\pi^2 E}{2(\nu^2-1)}\left[4(\nu-3)\sin(2\pi x)\sin(2\pi y) + (\nu+1)\cos(\pi x)\cos(\pi y)\right] = \; -f_x \;.$$

In the Y direction, using equations (4.3) and (4.4) we get,

$$\frac{\partial\sigma_{yy}}{\partial y} + \frac{\partial\sigma_{xy}}{\partial x} \;=\; -\frac{\pi^2 E}{2(\nu^2-1)}\left[4\,(\nu+1)\cos(2\pi x)\cos(2\pi y) + (\nu-3)\sin(\pi x)\sin(\pi y)\right] = \; -f_y \;.$$

Note that we had excluded body forces in our scheme. Plugging in the exact solution for stress, we have a non-zero body force density $\boldsymbol{f} = [f_x \;\; f_y]^T$. This, has to be taken into account in the scheme. The body force can be obtained by integrating the above equations over the local domain. We also have to ensure that we use the same displacement functions u^h and v^h to enforce the above equations (conservation laws). However, since the limits of each element is different, we must find a generic expansion for the element e over $\Omega_e = [x_i \;\; x_{i+1}] \times [y_j \;\; y_{j+1}]$ with coordinates (x, y). Under these circumstances, we have the basis function for displacement in the X direction,

$$u^h(x,y) = u^1 \frac{1}{2}\left(\frac{(1+\sqrt{3})x_{i+1} - (1-\sqrt{3})x_i - 2\sqrt{3}x}{x_{i+1}-x_i}\right) + u^2 \frac{1}{2}\left(\frac{(1-\sqrt{3})x_{i+1} - (1+\sqrt{3})x_i + 2\sqrt{3}x}{x_{i+1}-x_i}\right)$$

which imposes linear equilibrium in the X direction,

$$\int_{y_j}^{y_{j+1}} \int_{x_i}^{x_{i+1}} u^h \{-f_x\} \, \mathrm{d}x\mathrm{d}y \, .$$

The same way, we have the basis function for displacement in the Y direction,

$$v^h(x,y) = v^1 \frac{1}{2}\left(\frac{(1+\sqrt{3})y_{j+1} - (1-\sqrt{3})y_j - 2\sqrt{3}y}{y_{j+1}-y_j}\right) + v^2 \frac{1}{2}\left(\frac{(1-\sqrt{3})y_{j+1} - (1+\sqrt{3})y_j + 2\sqrt{3}y}{y_{j+1}-y_j}\right)$$

which imposes linear equilibrium in the Y direction,

$$\int_{y_j}^{y_{j+1}} \int_{x_i}^{x_{i+1}} v^h \{-f_y\} \, \mathrm{d}x\mathrm{d}y \, .$$

In our analytical solution, $\sigma_{yx} = \sigma_{xy}$ and hence there will be no body force terms emerging from conservation of angular momentum as shown in equation (3.9). Next,we must also check if there will be any non-zero displacements prescribed on the boundary of the domain Γ due to the fields u and v in equation (4.1). If we take our physical domain to be $[-1 \quad 1]^2$, multiple elements are packed inside this domain. It can be easily shown that the prescribed displacements on the boundary are zero because they vanish at the boundary points, $x = -1, x = 1, y = -1, y = 1$.

4.1 Qualitative analysis

For the normal stress σ_{xx}, first, contour plots will be presented and analysed. The colour code matches really well and the values get closer when the grid is refined. The approximate expansions for normal stress σ^h_{xx} are unable to mimic the contours attained by the exact solution. This is expected since the polynomial has a quadratic variation in the X direction and is constant in the Y direction (this is in good agreement with the images because discontinuous jumps are seen only in the Y direction). The

exact solution from equation (4.2) shows that there is variation in both directions, X and Y. This is the reason why ribbons are seen to appear in the plots. For a 20×20 grid, the patterns match more closely and for an even finer grid, really good results are expected.

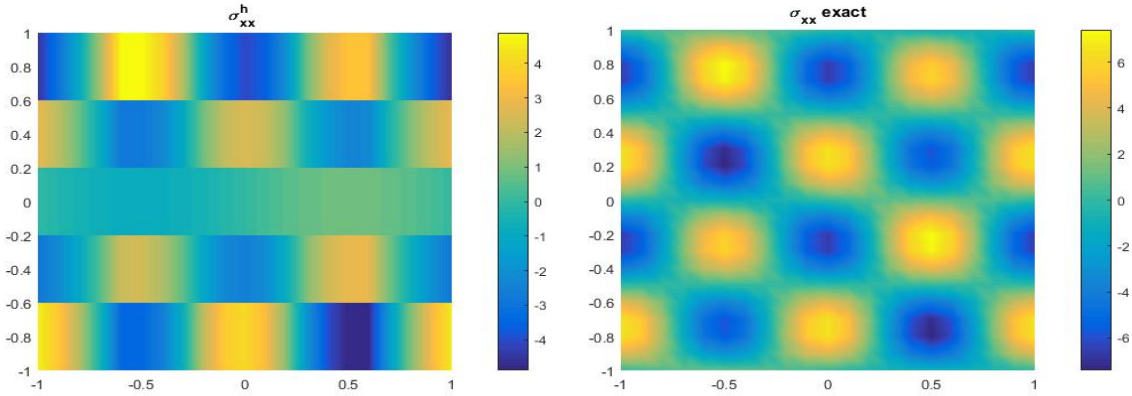

(a) Approximate σ^h_{xx} (b) Exact σ^h_{xx}

Figure 4.1: Normal stress σ_{xx} on a 5×5 grid

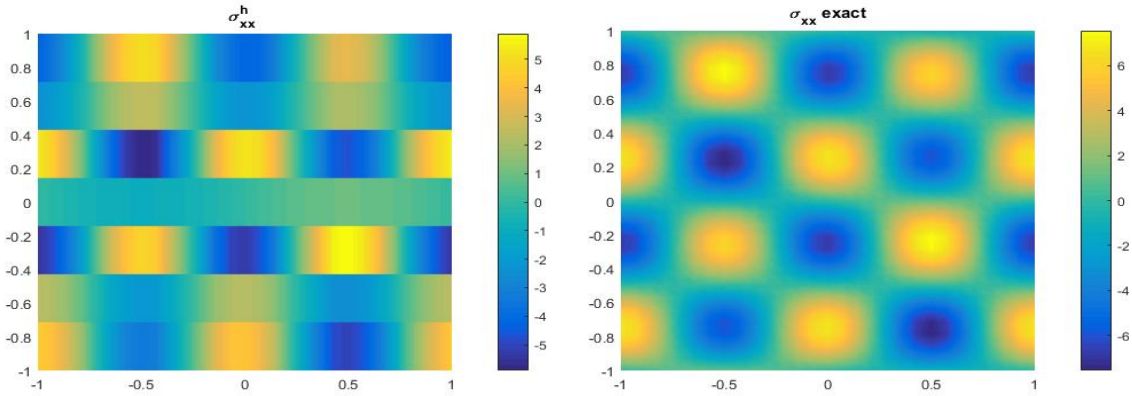

(a) Approximate σ^h_{xx} (b) Exact σ_{xx}

Figure 4.2: Normal stress σ_{xx} on a 7×7 grid

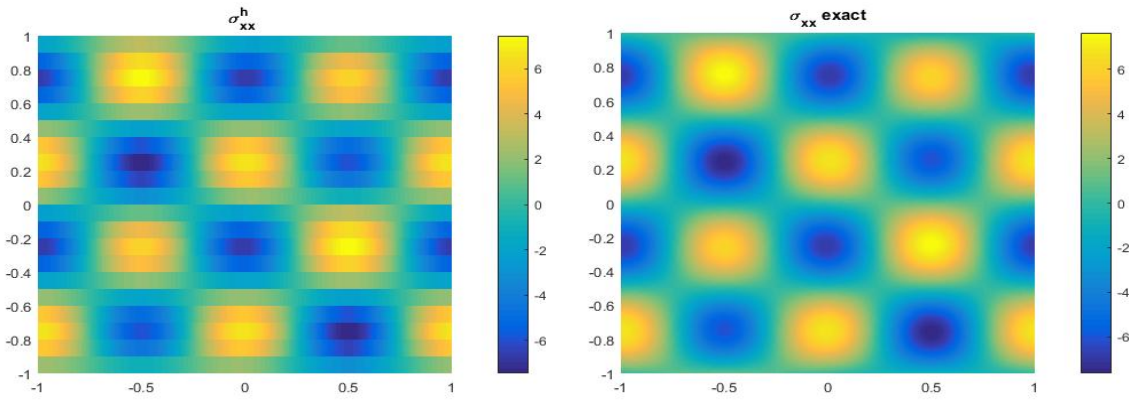

(a) Approximate σ^h_{xx} (b) Exact σ_{xx}

Figure 4.3: Normal stress σ_{xx} on a 20×20 grid

It is also beneficial to compare surface plots of the two as shown in Figure 4.4. A 20×20 mesh was chosen for this plot and the peaks are accurate. The variation in the X direction is clear; however, in the Y direction, each of these fields are like individual, separate layers. This is because our expansions are constant in the Y direction while the exact solution varies in both directions.

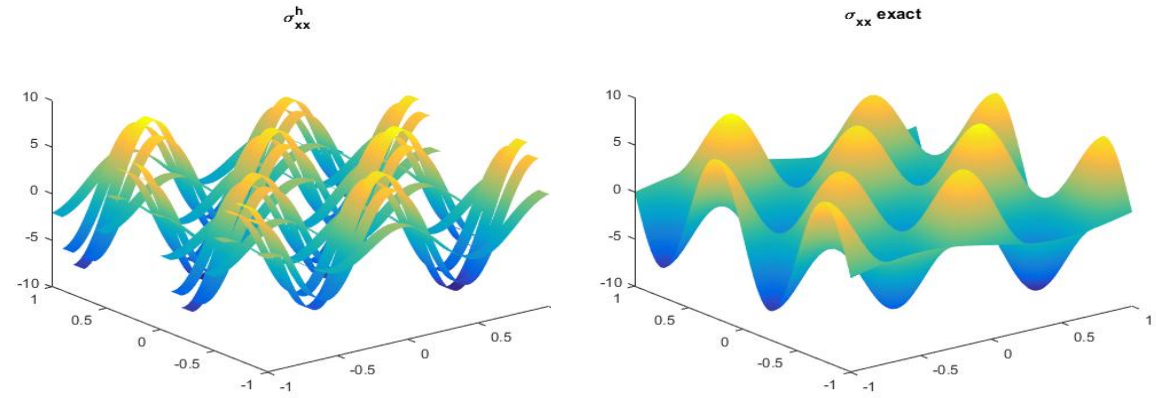

(a) Approximate σ^h_{xx} (b) Exact σ_{xx}

Figure 4.4: Surface plot for normal stress σ_{xx} on a 20×20 grid

The results of σ^h_{yy} are similar to normal stress σ^h_{xx} since the same kind of variation is used but in the orthogonal direction. Again, the values and colour maps match closely and a great improvement is seen in the contours for a 20×20 grid. The surface plot shown in Figure 4.8 portrays that the results are close. The approximate solution is

accurate but is again in the form of ribbons due to the invariance in the X direction.

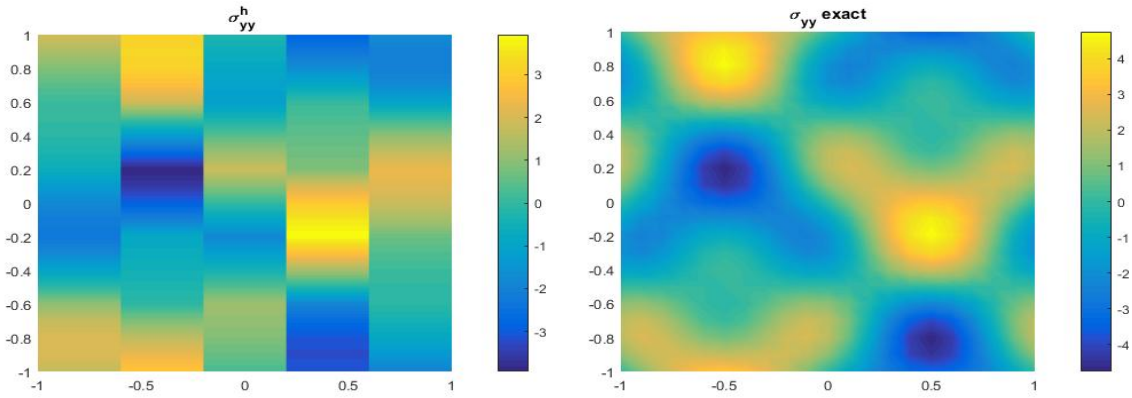

(a) Approximate σ^h_{yy} (b) Exact σ^h_{yy}

Figure 4.5: Normal stress σ_{yy} on a 5×5 grid

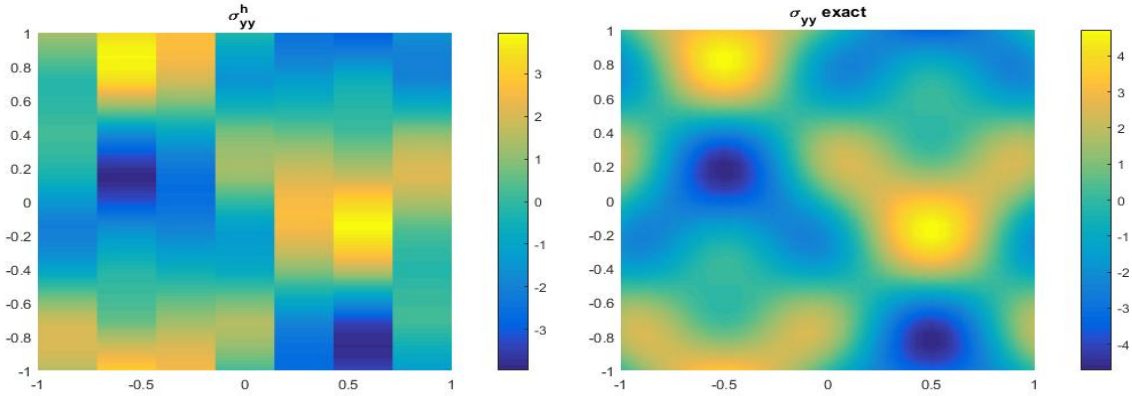

(a) Approximate σ^h_{yy} (b) Exact σ^h_{yy}

Figure 4.6: Normal stress σ_{yy} on a 7×7 grid

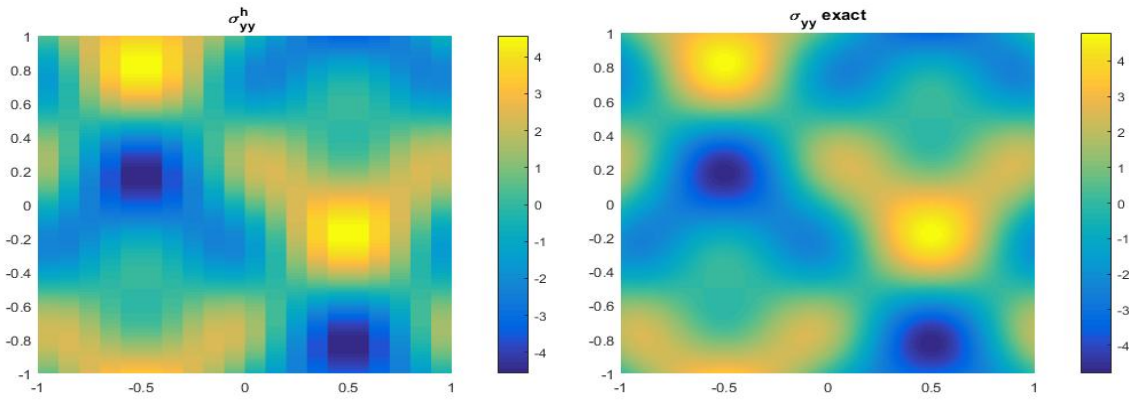

(a) Approximate σ^h_{yy} (b) Exact σ^h_{yy}

Figure 4.7: Normal stress σ_{yy} on a 20×20 grid

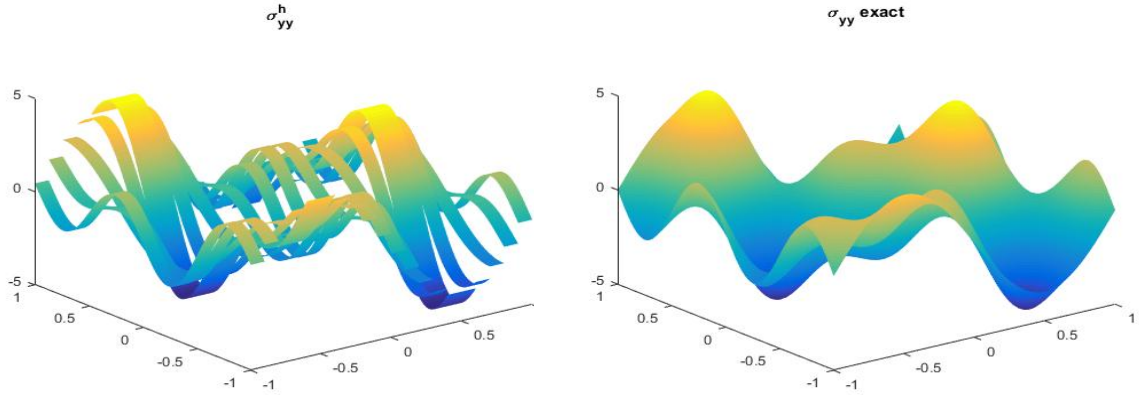

(a) Approximate σ^h_{yy} (b) Exact σ_{yy}

Figure 4.8: Surface plot for normal stress σ_{yy} on a 20×20 grid

For the shear stress, both the colours and the contours match nicely with mesh refinement. There are no discontinuous jumps because the approximate solutions varies linearly in both the X and Y direction. Once again, the solution is post-processed over the same grids taken for the normal stresses. Despite using lower order polynomials to try and catch the feature of the exact trigonometric functions, the results begin to mimic the contours greatly with mesh refinement.

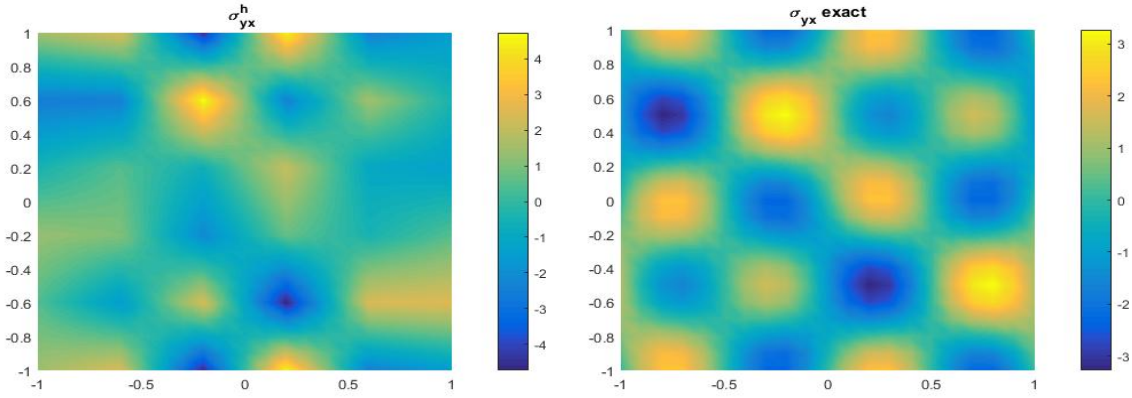

(a) Approximate σ^h_{yx} (b) Exact σ_{yx}

Figure 4.9: Shear stress σ_{yx} on a 5×5 grid

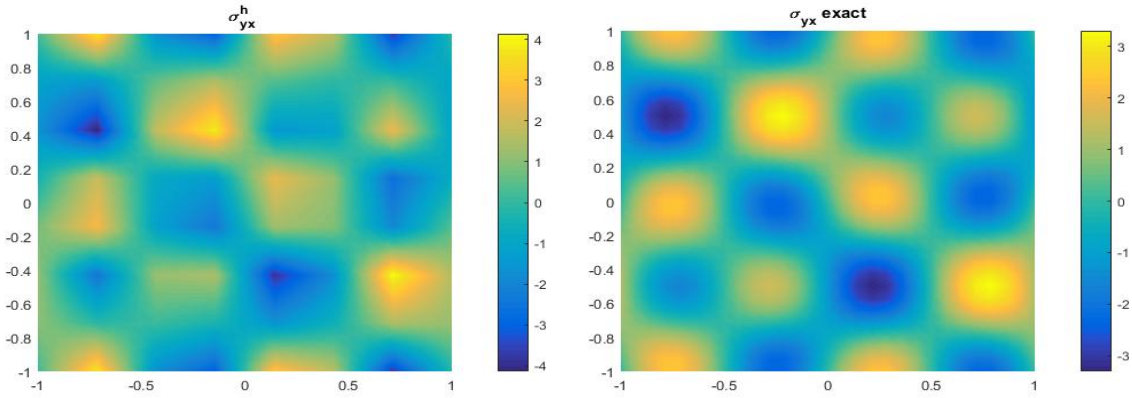

(a) Approximate σ^h_{yx} (b) Exact σ_{yx}

Figure 4.10: Shear stress σ_{yx} on a 7×7 grid

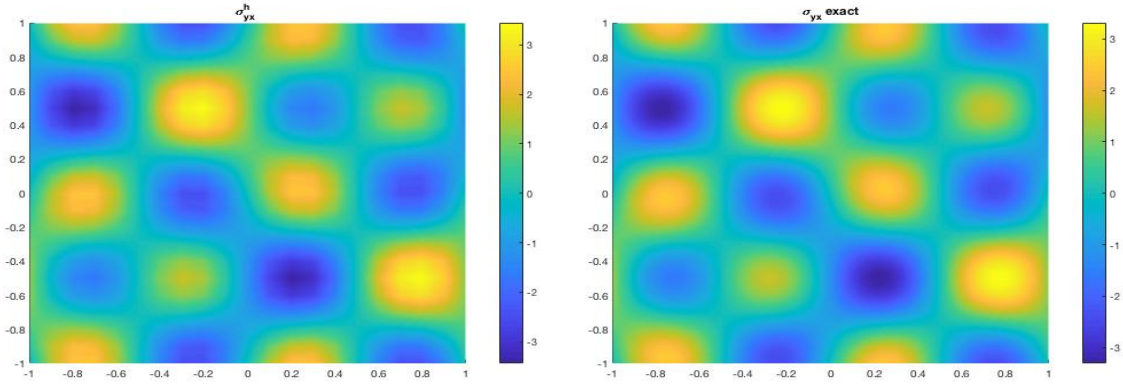

(a) Approximate σ^h_{yx} (b) Exact σ_{yx}

Figure 4.11: Shear stress σ_{yx} on a 20×20 grid

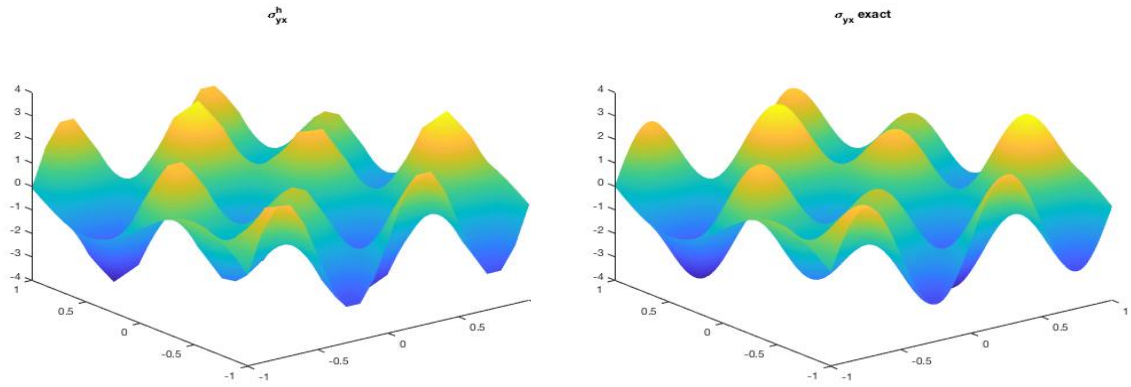

(a) Approximate σ_{yx}^h (b) Exact σ_{yx}

Figure 4.12: Surface plot for shear stress σ_{yx} on a 20×20 grid

For the exact solution, $\sigma_{xy} = \sigma_{yx}$ as shown in equation (4.4). For the approximate solutions, we impose them to be equal but they still have to be compared. The contours and surface plots look identical as shown in Figure 4.13 and 4.14. This means that the rotation field $\boldsymbol{\omega}^h$ which is the Lagrange multiplier successfully imposes symmetry of the stress tensor.

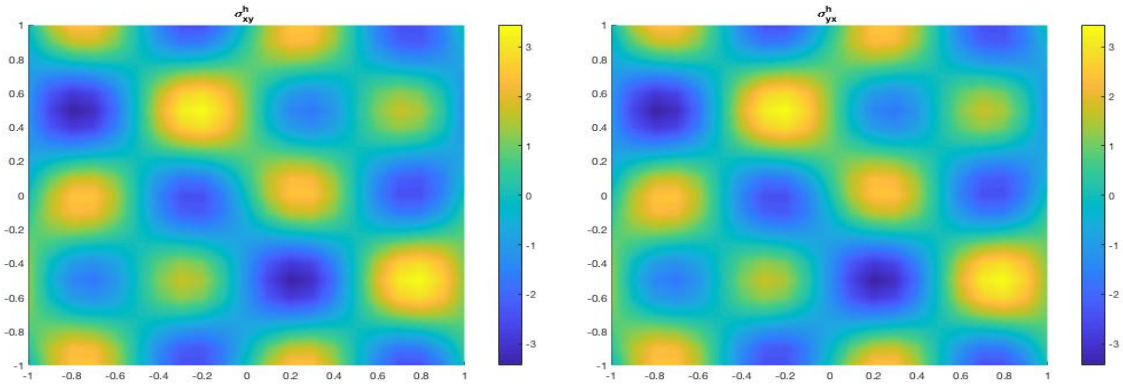

(a) Approximate σ_{xy}^h (b) Approximate σ_{yx}^h

Figure 4.13: Comparison of σ_{yx} and σ_{xy} on a 20×20 grid

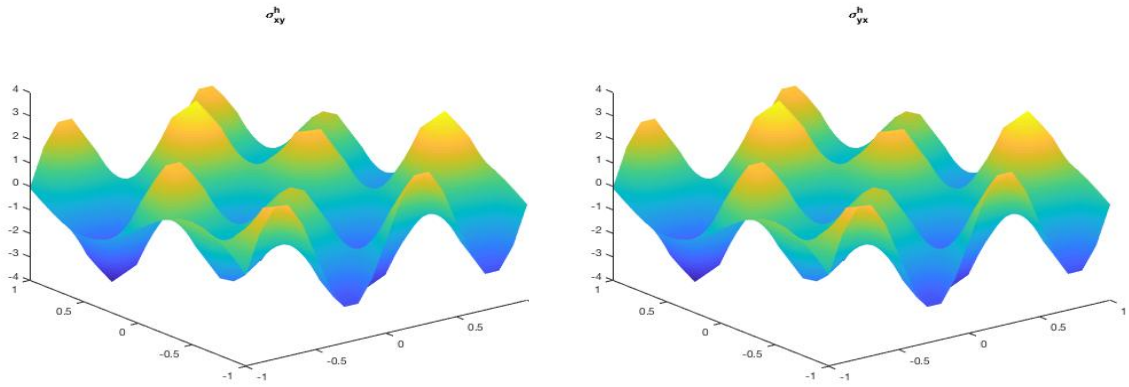

(a) Approximate σ^h_{yx} (b) Approximate σ^h_{xy}

Figure 4.14: Surface plot comparison of σ_{yx} and σ_{xy} on a 20×20 grid

This quantitative analysis shows that despite having a singular system, the solutions for stress remain unperturbed. However, results for kinematic modes like displacement and rotation will be meaningless due to the presence of SKMs. In the following subsection, a new method is proposed and attempted that helps in the removal of SKMs and yielding a non-singular system.

4.1.1 Attempt for a non-singular system

An idea is proposed in this section to circumvent the singularities generated at the internal corners where elements meet. Figure 4.15 shows that at the internal corner where the 4 elements meet, a dummy variable for shear stress σ_C has been introduced. Similarly, there are dummy variables introduced at the boundary of the domain; σ_L, σ_R, σ_B and σ_T. At the internal corner, we impose 4 equality constraints, $\sigma_1 = \sigma_C$, $\sigma_2 = \sigma_C$, $\sigma_3 = \sigma_C$ and $\sigma_4 = \sigma_C$ each of which is enforced by a single Lagrange multiplier. Similarly, for each of the external corners, there will be 2 equality constraints. Recalling that each element has a domain $[0\ h_1] \times [0\ h_2]$, we can evaluate the shear stress at each corner.

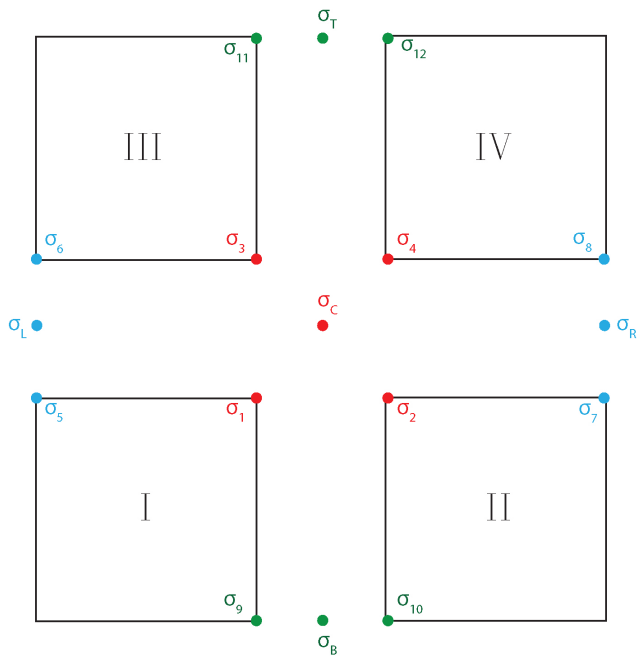

Figure 4.15: Imposing shear stress continuity

For the internal corner,

$$\sigma_1 \;=\; \sigma^I_{yx}(x_{i+1}, y_{j+1}) \;=\; \frac{3T^4_{yx} - T^2_{yx}}{h_1} \;=\; \sigma_C \;,$$

$$\sigma_2 \;=\; \sigma^{II}_{yx}(x_i, y_{j+1}) \;=\; \frac{3T^2_{yx} - T^4_{yx}}{h_1} \;=\; \sigma_C \;,$$

$$\sigma_3 \;=\; \sigma^{III}_{yx}(x_{i+1}, y_j) \;=\; \frac{3T^3_{yx} - T^1_{yx}}{h_1} \;=\; \sigma_C \;,$$

$$\sigma_4 \;=\; \sigma^{IV}_{yx}(x_i, y_j) \;=\; \frac{3T^1_{yx} - T^3_{yx}}{h_1} \;=\; \sigma_C \;.$$

These constraints must be enforced by Lagrange multipliers l_i such that,

$$l_1(\sigma_1 - \sigma_C) \;+\; l_2(\sigma_2 - \sigma_C) \;+\; l_3(\sigma_3 - \sigma_C) \;+\; l_4(\sigma_4 - \sigma_C) \;=\; 0 \;.$$

Taking variations with respect to σ_C , we get an equation for the Lagrange multipliers,

$$-l_1 \;-\; l_2 \;-\; l_3 \;-\; l_4 \;=\; 0 \;,$$

which should remove the singularity. The same technique is applied to the external boundary of the domain. For example, at the left boundary, we impose,

$$m_1(\sigma_5 - \sigma_L) \; + \; m_2(\sigma_6 - \sigma_L) \; = \; 0 \; ,$$

where,

$$\sigma_5 \; = \; \sigma^I_{yx}(x_i, y_{j+1}) \; = \; \frac{3T^2_{yx} - T^4_{yx}}{h_1} \; = \; \sigma_L \; ,$$

$$\sigma_6 \; = \; \sigma^{III}_{yx}(x_i, y_j) \; = \; \frac{3T^1_{yx} - T^3_{yx}}{h_1} \; = \; \sigma_L \; ,$$

Once again, taking variations with respect to the dummy variable σ_L, we get the equation for the Lagrange multipliers m_i,

$$-m_1 \; - \; m_2 \; = \; 0 \; .$$

Hence, in our matrix, we will have equations for all the constraints and the Lagrange multipliers satisfying these constraints. Implementing this method for all corners works perfectly and yields a **non-singular** system and hence guarantees a unique solution! Note that this same procedure need not be performed for σ_{xy} since we explicitly impose symmetry of stress tensor ($\sigma_{xy} \; = \; \sigma_{yx}$). The fact that the scheme is free of SKMs is really good news. The post-processing showed the same results for the stress fields and now physical results for the displacement fields! As opposed to the analytical rotation field $\boldsymbol{\omega}$, the Lagrange multiplier $\boldsymbol{\omega}^h$ that imposes symmetry of stress tensor is wayward and discontinuous. The kinematic results are now shown in Figures 4.16, 4.17, 4.18 and 4.19. The ribbons in the plots for displacements occur since the polynomials have linear variation only in one direction.

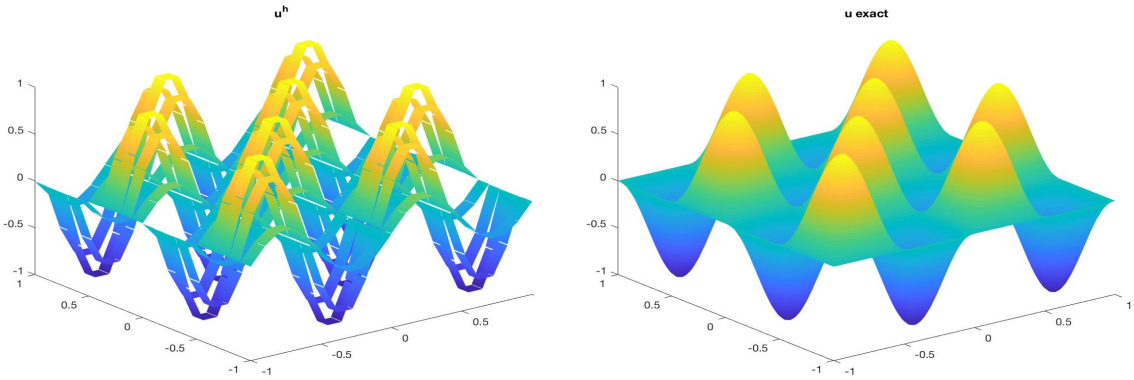

(a) Approximate displacement u^h (b) Exact displacement u

Figure 4.16: Surface plot for the X component of displacement on a 20×20 grid

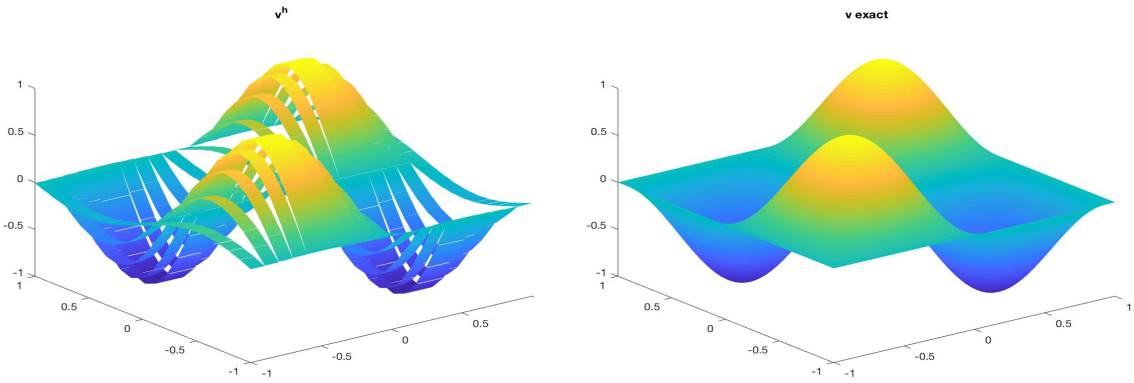

(a) Approximate displacement v^h (b) Exact displacement v

Figure 4.17: Surface plot for the Y component of displacement on a 20×20 grid

The results for $\boldsymbol{\omega}^h$ are very strange. The contour plots show continuity in the Y direction but there are large discontinuous leaps in the X direction. Also, the degrees of freedom ω^i were seen to increase as step size decreased, thereby causing an amplification of the overall value of the rotation field ω^h.

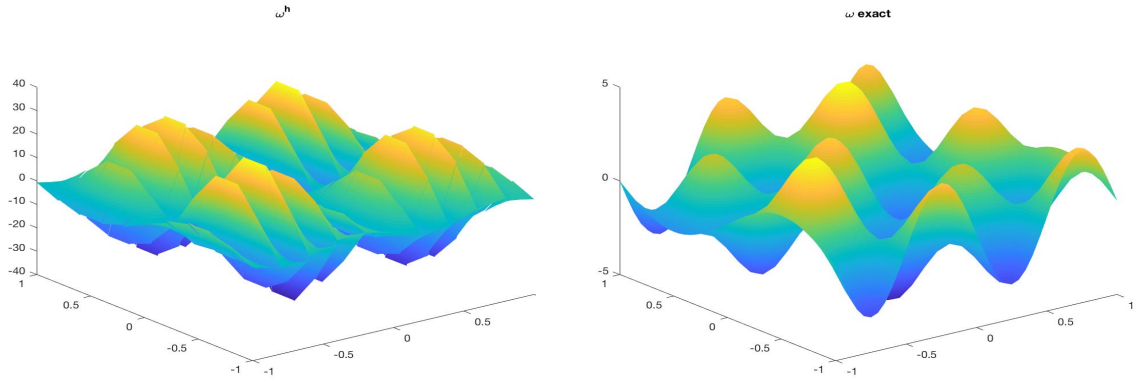

(a) Approximate rotation ω^h (b) Exact rotation ω

Figure 4.18: Surface plot for rotation on a 10×10 grid

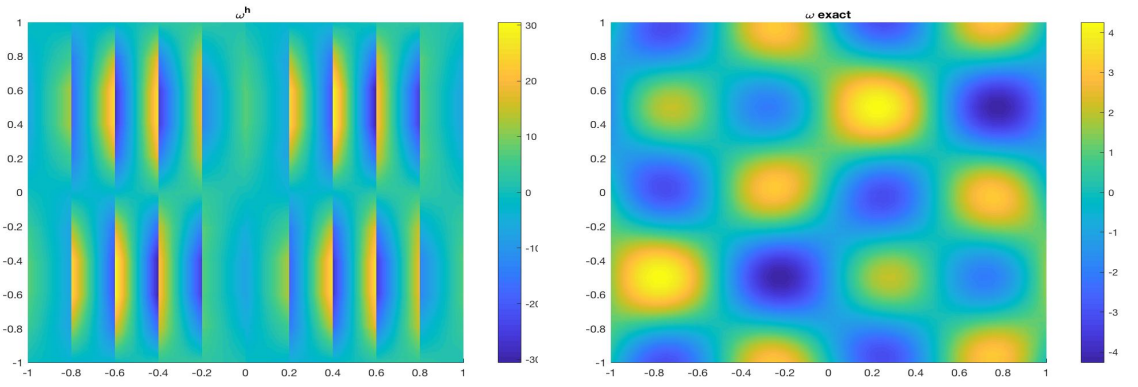

(a) Approximate rotation ω^h (b) Exact rotation ω

Figure 4.19: Contour plot for rotation on a 10×10 grid

4.2 Quantitative analysis

In this section, we want to see how well the solutions converge (for the method generating the non-singular system), if they do. For this, we compute the error in the $L^2(\Omega)$ norm for all the stress components, displacements and rotation field. The error in the $L^2(\Omega)$ norm for a function ψ is given by,

$$\|\psi^h - \psi^e\|_{L^2(\Omega)} = \sqrt{\int_\Omega (\psi^h - \psi^e)^2 \, \mathrm{d}\Omega} \ ,$$

where the superscripts h and e denote the approximate and exact solution respectively for the function ψ. The performance of the scheme for stresses and kinematic variables are shown in Figure 4.20 and Figure 4.21.

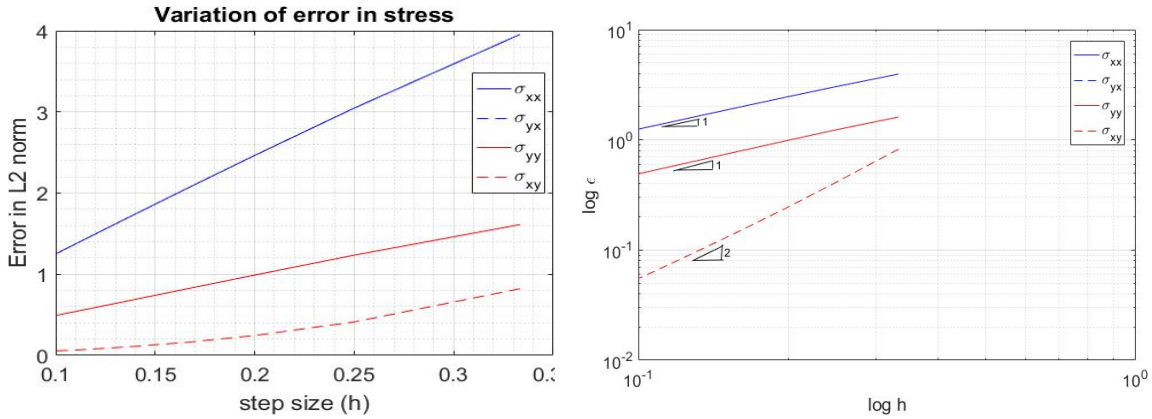

(a) Error in the L^2 norm (b) log-log plot for convergence of stress

Figure 4.20: Error analysis for stresses

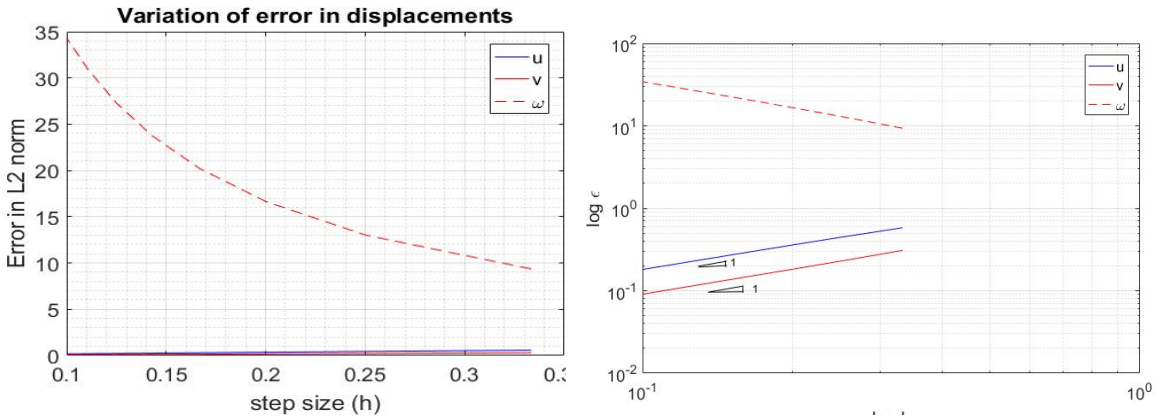

(a) Error in the L^2 norm (b) log-log plot for convergence of stress

Figure 4.21: Error analysis for kinematic variables

For a smooth solution with a polynomial degree $\mathcal{N}$, we expect a convergence rate of $\mathcal{O}(h^{\mathcal{N}+1})$, [22]. For the normal stress, we have a quadratic variation in one direction and no variation in the orthogonal direction. Hence, the lowest degree of the polynomial is $\mathcal{N} = 0$ and a convergence rate of $\mathcal{O}(h)$ is optimal. The same rate is expected for displacements due to linear variation in one direction and no variation in the other. For shear stresses and rotation, due to the linear variation in both directions, we expect a convergence rate of $\mathcal{O}(h^2)$. Checking the results, the slopes for normal stresses

and displacements converge to 1 while for the shear stress, the slope converges to 2. However, for rotation, the results are incorrect as we expect from the qualitative analysis. The error seems to be diverging very rapidly. Overall, the results shows that we have optimal convergence for stresses and displacement while the rotation is certainly nonphysical and discontinuous.

Chapter 5

Conclusions and future work

Firstly, this report highlights the investigation of mixed an hybrid finite element formulations as the motivation of the project. After discussing the advantages and drawbacks of the mixed formulations with the help of the Poisson problem in $\mathbb{R}^1$, some concepts in linear elasticity are mentioned. Using linear elasticity as a base, an attempt is then made to develop a hybrid finite element scheme.

After testing a single element, we moved to multiple elements where the importance of applying the interface potential was discussed. This result however, produced a singular system with Spurious Kinematic Modes (SKMs), a totally expected scenario in such formulations. Still, the system was evaluated for a test cases in 2D linear elasticity involving manufactured solutions for the displacement fields. From this, we obtained the analytical strains using compatibility relations and stresses using constitutive relations. While solving the hybrid system did not affect the approximate stress fields, it was not ideal because physical results for kinematic fields were desired. For this, a new method was proposed that led to a non-singular system free of SKMs! The research question was whether a finite element scheme could be devised that is free of SKMs. We have a positive answer for the research question,

Yes, a finite element scheme free of Spurious Kinematic Modes (SKMs) is achieved.

The idea was to then verify the code and evaluate the performance and convergence of the scheme. The solution for stress fields and displacement fields are obtained

throughout the domain. *Optimal convergence* was achieved for all the components of the stress field and displacement field. For now, it is clear that the Lagrange multiplier $\boldsymbol{\omega}^h$ imposes symmetry of stress tensor. It is recommended that in the future, this Lagrange multiplier is investigated for its physical significance. From the theoretical perspective, it is supposed to be the rotation field but the results show otherwise.

The use of lower-order polynomials limits the convergence rate of the scheme. In the future, it is recommended to work with higher order polynomials and compare results. They should be able to mimic the contours and surface plots much better. Once some higher order polynomials are tested, it is advised to move to deformed meshes to check if conservation laws still hold. The matrix structure used in equation (3.42) for the hybrid scheme has certain nice properties. Firstly, most of the matrix is sparse. The second good point is that the arrangement of the entries for matrix $\mathcal{M}$ is element by element and in a diagonal setting. This can be very useful because computations can be made in a parallel way; that is, each elemental matrix can be solved separately without dealing with the entire system in (3.42). This is one of the main motivations for using the hybrid formulation despite having to face SKMs in the scheme. For example, we have,

$$\begin{pmatrix} \mathcal{A} & \mathcal{B}^T \\ \mathcal{B} & 0 \end{pmatrix} \begin{bmatrix} \mathscr{U} \\ \mathscr{P} \end{bmatrix} = \begin{bmatrix} \mathcal{F} \\ \mathcal{K} \end{bmatrix}, \tag{5.1}$$

where $\mathcal{A}$ represents the elemental matrices $\mathcal{G}$ in equation (3.42) stacked diagonally. Note that it is very (computationally) cheap to compute the inverse of $\mathcal{A}$. We multiply this system with $\mathcal{A}^{-1}$ and we have,

$$\begin{pmatrix} \mathbb{I} & \mathcal{A}^{-1}\mathcal{B}^T \\ \mathcal{B} & 0 \end{pmatrix} \begin{bmatrix} \mathscr{U} \\ \mathscr{P} \end{bmatrix} = \begin{bmatrix} \mathcal{A}^{-1}\mathcal{F} \\ \mathcal{K} \end{bmatrix}.$$

Performing row operations,

$$\begin{pmatrix} \mathbb{I} & \mathcal{A}^{-1}\mathcal{B}^T \\ 0 & -\mathcal{B}\mathcal{A}^{-1}\mathcal{B}^T \end{pmatrix} \begin{bmatrix} \mathscr{U} \\ \mathscr{P} \end{bmatrix} = \begin{bmatrix} \mathcal{A}^{-1}\mathcal{F} \\ \mathcal{K} - \mathcal{B}\mathcal{A}^{-1}\mathcal{F} \end{bmatrix}.$$

We work on finding $\mathscr{P}$ using,

$$-\mathcal{B}\mathcal{A}^{-1}\mathcal{B}^{T}\ \mathscr{P}\ =\ \mathcal{K}-\mathcal{B}\mathcal{A}^{-1}\mathcal{F}\ . \tag{5.2}$$

$\mathscr{P}$ can be solved using an iterative sub-structuring process with the FETI (Finite Element Tearing and Interconnecting) method, [23]. Once this is done, there is no need of solving the entire system. The vector containing the unknown fields $\mathscr{U}$ can be found,

$$\mathbb{I}\,\mathscr{U}\ +\ \mathcal{A}^{-1}\mathcal{B}^{T}\mathscr{P}\ =\ \mathcal{A}^{-1}\mathcal{F}$$

or simply,

$$\mathscr{U}\ =\ \mathcal{A}^{-1}\left[\mathcal{F}\ -\ \mathcal{B}^{T}\mathscr{P}\right]\ . \tag{5.3}$$

In the report, $\mathscr{P}$ is the vector of Lagrange multipliers Φ. If we solve for this, it is really very efficient to compute our system for large number of cells. Therefore, doing more research and working with FETI techniques can be very beneficial. These schemes have also been found to be independent of the number of unknowns involved in the system [1].

5.1 Possible extension to fluid dynamics

To cope with the growing demand of more efficient and reliable wind energy generation, vortex generators (VGs) have been tested on wind turbine blades. As the name suggests, these small devices generate streamwise vortical structures when there is air flow over the surface. The vortices energise the flow by circulating high-momentum outer flow over the slow moving boundary layers close to the aerofoil surface thereby delaying flow separation and aerodynamic stall. An experimental study, [24] depicts a sharp increase in efficiency (by increasing lift) with the addition of VGs as shown in figure 5.1.

[1] Marc Gerritsma, Associate Professor, Aerospace engineering, Delft University of Technology.

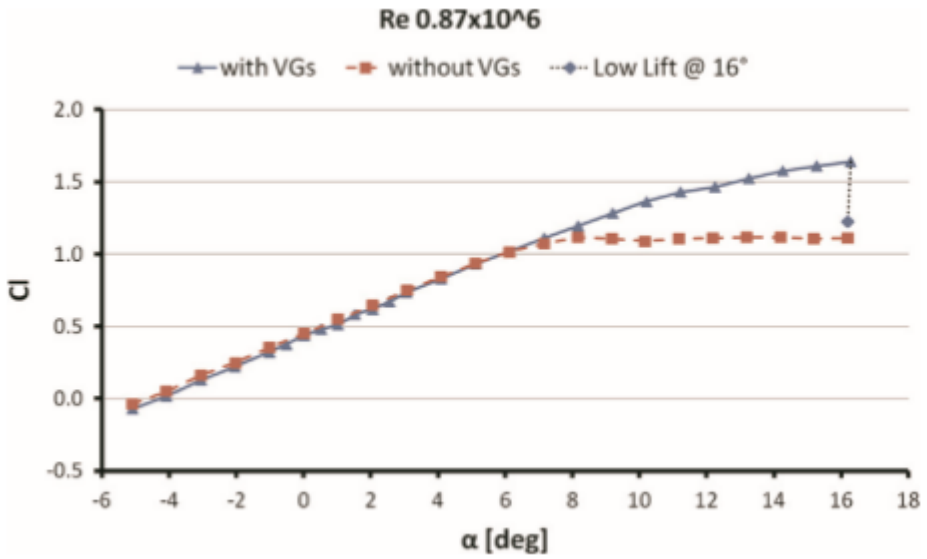

Figure 5.1: Effect of VGs on lift coefficient C_L, [24]

One cannot solely rely on experiments however and computational studies are always sought. The size of VGs are extremely small compared to the size of the blade. Furthermore, in order to capture the complicated flow physics associated with VGs accurately, one has to work with a very fine computational mesh. For the reasons mentioned, setting up a computational model can be very challenging and expensive. To circumvent this problem , [28] models a crucial effect of the VG on the flow (in terms of a body force term in the Navier-Stokes equation) which triggers vortex generation instead of including the geometry of the VG itself. A source term that provided an optimal match in the *velocity field* on a course mesh was deemed sufficient in yielding accurate results. The approach intended in the future has a different direction, however. The approach in [28], involves the use of Finite Volume methods (FVM) while the future project intends to work with Mixed and Hybrid Formulations. The mixed finite element formulation is not very easy to implement due to the rigour involved in choosing appropriate function spaces as was shown in chapter 2 for a relatively much simpler problem.

A source term that provides an optimal match in the (symmetric part of the) rate of strain tensor is sought; subject to fluid dynamic constraints. Consider a functional $\mathcal{J}$ that is to be minimised. One of its key components is the (symmetric part) rate of strain tensor, which is given by,

$$D_{ij}\left(\boldsymbol{u}\right) = \frac{1}{2}\left(\frac{\partial u_i}{\partial x_j} + \frac{\partial u_j}{\partial x_i}\right) \ .$$

If $\bar{\boldsymbol{u}}$ is the target solution supplemented with experimental results or from a highly refined mesh and $\boldsymbol{u}$ is the required solution (velocity field) on a course mesh, we need,

$$D(\boldsymbol{u}) - D(\bar{\boldsymbol{u}}) = 0 \ . \tag{5.4}$$

A *sufficient condition* for equation (5.4) to be zero would be to have $\boldsymbol{u} = \bar{\boldsymbol{u}}$. To achieve a *unique* solution suited to our purpose however, there must be an additional constraint(s) at the very least. A constraint that will be used is the incompressibility condition from fluid dynamics,

$$\nabla \cdot \boldsymbol{u} = 0 \ .$$

Writing this as a variational problem in the Hilbert space (Appendix B), we have,

$$\inf_{\boldsymbol{v} \in V} \mathcal{J}(\boldsymbol{v}) \ ,$$

where $\mathcal{J}(.)$ is a functional and V is a finite dimensional space. When it is differentiable, the minimum is characterised by a variational equation, [5],

$$\langle J'(\boldsymbol{u}), \boldsymbol{v} \rangle_{V' \times V} = 0 \qquad \forall \boldsymbol{v} \in V \ ,$$

where $\langle ., . \rangle_{V' \times V}$ denotes duality pairing between vector space V and its dual space V'. The complete variational problem must also contain the constraints mentioned, enforced by Lagrange multipliers. Consider a smooth, closed domain Ω bounded by $\Gamma(\Omega)$ such that,

$$\mathcal{L}(\boldsymbol{u}, \underset{\approx}{\sigma}, p) \ = \ \underbrace{\frac{1}{2}\int_\Omega D(\boldsymbol{u}) : D(\boldsymbol{u}) \ \mathrm{d}\Omega}_{\mathcal{J}(\boldsymbol{u})} \ + \ \int_\Omega \left(D(\boldsymbol{u}) - D(\bar{\boldsymbol{u}})\right) : \underset{\approx}{\sigma} \ \mathrm{d}\Omega \ + \ \int_\Omega \left(\nabla \cdot \boldsymbol{u}\right) p \ \mathrm{d}\Omega \ , \tag{5.5}$$

In equation (5.5), $\mathcal{L}(\boldsymbol{u}, \underset{\approx}{\sigma}, p)$ is the Lagrangian and the Lagrange multipliers ($\underset{\approx}{\sigma}$ and p) ensure that the corresponding constraints are enforced correctly. Here, σ has a notation $\underset{\approx}{\sigma}$ because it is a tensor and p, which is a scalar, represents pressure. Note that there are as many multipliers as there are constraints. Taking Gâteaux variations with respect to each variable of the Lagrangian and equating them to zero, balances the system. Before we take the derivatives, the variables of the Lagrangian are perturbed as $\boldsymbol{u} + \epsilon\tilde{\boldsymbol{u}}$, $\underset{\approx}{\sigma} + \gamma\underset{\approx}{\tilde{\sigma}}$ and $p + \delta\tilde{p}$. After this, we are left with,

$$\int_\Omega D(\boldsymbol{u}) : D(\tilde{\boldsymbol{u}}) \ \mathrm{d}\Omega \ + \ \int_\Omega D(\tilde{\boldsymbol{u}}) : \underset{\approx}{\sigma} \ \mathrm{d}\Omega \ + \ \int_\Omega (\nabla \cdot \tilde{\boldsymbol{u}})\, p \ \mathrm{d}\Omega \ = \ 0 \qquad \forall \tilde{\boldsymbol{u}} \in H^1(\Omega) \ , \tag{5.6}$$

$$\int_\Omega (D(\boldsymbol{u}) - D(\bar{\boldsymbol{u}})) : \underset{\approx}{\tilde{\sigma}} \ \mathrm{d}\Omega \ = \ 0 \qquad \forall \underset{\approx}{\tilde{\sigma}} \in L^2(\Omega) \ , \tag{5.7}$$

$$\int_\Omega (\nabla \cdot \boldsymbol{u})\, \tilde{p} \ \mathrm{d}\Omega \ = \ 0 \qquad \forall \tilde{p} \in L^2(\Omega) \ . \tag{5.8}$$

It is important to realise that this system has no boundary conditions at the moment; or they are hidden behind the scenes. Boundary conditions can be applied through the boundary integral terms that can arise through simplification and/or integration by parts. To avoid too many terms, we want to work in $\mathbb{R}^2$. This way, there are lesser components for vector and tensor fields. Let the velocity field $\boldsymbol{u} = [u, \ v]^T$. We work with the first term of equation (5.6) and try to simplify it,

$$\begin{aligned}
\int_\Omega D(\boldsymbol{u}) : D(\tilde{\boldsymbol{u}}) \ \mathrm{d}\Omega \ &= \ \int_\Omega \frac{\partial u}{\partial x}\frac{\partial \tilde{u}}{\partial x} \ + \ \frac{1}{2}\left(\frac{\partial u}{\partial y} \ + \ \frac{\partial v}{\partial x}\right)\left(\frac{\partial \tilde{u}}{\partial y} \ + \ \frac{\partial \tilde{v}}{\partial x}\right) \ + \ \frac{\partial v}{\partial y}\frac{\partial \tilde{v}}{\partial y} \ \mathrm{d}\Omega, \\
&= \underbrace{\int_\Gamma \frac{\partial u}{\partial x} \ \tilde{u} \cdot \hat{n}_x \mathrm{d}\Gamma}_{} - \int_\Omega \frac{\partial^2 u}{\partial x^2} \ \tilde{u}\mathrm{d}\Omega + \underbrace{\frac{1}{2}\int_\Gamma \left(\frac{\partial u}{\partial y} + \frac{\partial v}{\partial x}\right) \tilde{u} \cdot \hat{n}_y \mathrm{d}\Gamma}_{} - \frac{1}{2}\int_\Omega \frac{\partial}{\partial y}\left(\frac{\partial u}{\partial y} + \frac{\partial v}{\partial x}\right) \tilde{u} \ \mathrm{d}\Omega \\
&+ \underbrace{\frac{1}{2}\int_\Gamma \left(\frac{\partial u}{\partial y} + \frac{\partial v}{\partial x}\right) \tilde{v} \cdot \hat{n}_x \mathrm{d}\Gamma}_{} \ - \frac{1}{2}\int_\Omega \frac{\partial}{\partial x}\left(\frac{\partial u}{\partial y} + \frac{\partial v}{\partial x}\right) \tilde{v}\mathrm{d}\Omega \ + \ \underbrace{\int_\Gamma \frac{\partial v}{\partial y} \ \tilde{v} \cdot \hat{n}_y \mathrm{d}\Gamma}_{} - \int_\Omega \frac{\partial^2 v}{\partial y^2} \ \tilde{v}\mathrm{d}\Omega \ ,
\end{aligned} \tag{5.9}$$

where we have used integration by parts and Gauss Divergence Theorem. To simplify the system, we must work with the boundary integrals. Homogeneous or non-homogeneous boundary conditions can be prescribed strongly or weakly based on the

physical situation we are interested in and the terms involved in the integrals. Since this is a viscous problem, imposing the **no-slip condition** (tangential component of velocity is zero) and **no penetration condition** (normal component of velocity is zero) is preferred. These are strongly prescribed over Γ,

$$\begin{aligned} \boldsymbol{u}\cdot\hat{\boldsymbol{n}} = 0 \implies u\cdot\hat{n}_x \;+\; v\cdot\hat{n}_y = 0\,, \\ \boldsymbol{u}\times\hat{\boldsymbol{n}} = 0 \implies -u\cdot\hat{n}_y \;+\; v\cdot\hat{n}_x = 0\,. \end{aligned} \tag{5.10}$$

Equation (5.10) is possible if and only if $u = v = 0$ on Γ. This implies,

$$\boldsymbol{u} = 0 \quad \text{ on } \Gamma\,. \tag{5.11}$$

Since, $u = v = 0$, their perturbations $\tilde{u} = \tilde{v} = 0$. Hence, all the boundary integrals vanish and equation (5.9) is now simplified to,

$$= -\int_\Omega \frac{\partial^2 u}{\partial x^2}\;\tilde{u}\;\mathrm{d}\Omega \;-\; \frac{1}{2}\int_\Omega\left(\frac{\partial^2 u}{\partial y^2}+\frac{\partial^2 v}{\partial y\partial x}\right)\tilde{u}\;\mathrm{d}\Omega \;-\; \frac{1}{2}\int_\Omega\left(\frac{\partial^2 u}{\partial x\partial y}+\frac{\partial^2 v}{\partial x^2}\right)\tilde{v}\;\mathrm{d}\Omega - \int_\Omega \frac{\partial^2 v}{\partial y^2}\;\tilde{v}\mathrm{d}\Omega\,,$$

$$= -\frac{1}{2}\Bigg[\underbrace{\int_\Omega\left(\frac{\partial^2 u}{\partial x^2}+\frac{\partial^2 u}{\partial y^2}\right)\tilde{u}+\left(\frac{\partial^2 v}{\partial y^2}+\frac{\partial^2 v}{\partial x^2}\right)\tilde{v}\;\mathrm{d}\Omega}_{\int_\Omega \Delta\boldsymbol{u}\cdot\tilde{\boldsymbol{u}}\mathrm{d}\Omega} + \int_\Omega\left(\frac{\partial^2 u}{\partial x^2}+\frac{\partial^2 v}{\partial y\partial x}\right)\tilde{u}\;+\left(\frac{\partial^2 v}{\partial y^2}+\frac{\partial^2 u}{\partial x\partial y}\right)\tilde{v}\mathrm{d}\Omega\Bigg]\,,$$

$$= \;-\frac{1}{2}\left[\int_\Omega \Delta\boldsymbol{u}\cdot\tilde{\boldsymbol{u}}\;\mathrm{d}\Omega \;+\; \int_\Omega \frac{\partial}{\partial x}\underbrace{\left(\frac{\partial u}{\partial x}+\frac{\partial v}{\partial y}\right)}_{\nabla\cdot\boldsymbol{u}=0}\tilde{u} \;+\; \frac{\partial}{\partial y}\underbrace{\left(\frac{\partial v}{\partial y}+\frac{\partial u}{\partial x}\right)}_{\nabla\cdot\boldsymbol{u}=0}\tilde{v}\;\mathrm{d}\Omega\right].$$

Therefore,

$$\int_\Omega D(\boldsymbol{u}) : D(\tilde{\boldsymbol{u}})\;\mathrm{d}\Omega \;=\; -\frac{1}{2}\int_\Omega \Delta\boldsymbol{u}\cdot\tilde{\boldsymbol{u}}\;\mathrm{d}\Omega\,. \tag{5.12}$$

Working with the second and third terms of equation (5.6) it can also be shown that,

$$\int_\Omega D(\tilde{\boldsymbol{u}}) : \underset{\approx}{\sigma}\;\mathrm{d}\Omega \;=\; -\int_\Omega\left(\nabla\cdot\underset{\approx}{\sigma}\right)\cdot\tilde{\boldsymbol{u}}\;\mathrm{d}\Omega\,, \tag{5.13}$$

$$\int_\Omega (\nabla\cdot\tilde{\boldsymbol{u}})\,p\;\mathrm{d}\Omega = -\int_\Omega \nabla p\cdot\tilde{\boldsymbol{u}}\;\mathrm{d}\Omega\,. \tag{5.14}$$

where the symmetry of the stress tensor $\sigma_{ij} = \sigma_{ji}$ and boundary conditions were used to obtain equation (5.13) and (5.14). Combining these equations and using them in equation (5.6), we have,

$$\frac{1}{2}\int_{\Omega} \Delta \boldsymbol{u}\cdot\tilde{\boldsymbol{u}}\ \mathrm{d}\Omega\ +\ \int_{\Omega}\Big(\nabla\cdot\underset{\approx}{\sigma}\Big)\cdot\tilde{\boldsymbol{u}}\ \mathrm{d}\Omega\ +\ \int_{\Omega}\nabla p\cdot\tilde{\boldsymbol{u}}\ \mathrm{d}\Omega\ =\ 0 \qquad \forall\tilde{\boldsymbol{u}}\in H_0^1(\Omega)\ , \tag{5.15}$$

with equations (5.7) and (5.8) to complete the system; subject to the boundary condition (5.11). To summarise, we had an idea for an alternate representation of VGs to compute vortex induced flows. That led to a constrained minimisation problem, which we worked with by choosing suitable constraints. The variational analysis led to a system of equations subject to a physical Dirichlet boundary condition. This is the well known Variational Boundary Value Problem (VBVP) that can be solved with the help of finite element formulations. However, it is recommended that a more thorough analysis is performed in order to check the well-posedness of the problem before building a finite element scheme. If the number of constraints are not enough, the solution may not be unique; if there are too many constraints, the problem will be ill-posed. Another major challenge will be in dealing with many more unknown variables and hence more function spaces. Once we have a well-posed problem, the hybrid scheme will have the exact same structure; the mass matrix $\mathcal{M}$ will be related to the functional of the Lagrangian and the constraint matrices are placed adjacent to $\mathcal{M}$. Subsequently, continuity conditions can be imposed at the interfaces between elements.

Bibliography

[1] C. Lanczos, *The Variational Principles of Mechanics*, Mathematical Expositions, No. 4, University of Toronto, Reprinted in 1952.

[2] B. Daya Reddy, *Introductory Functional Analysis : With applications to Boundary Value Problems and Finite Elements*, Springer, Texts in Applied Mathematics, 27, ISBN 0-387-98307-4.

[3] *Advanced Variational Methods in Mechanics*, Chapter 13, Hybrid variational principles, University of Colorado at Boulder.

[4] J. P. Moitinho de Almeida, Edward. A. W. Maunder, *Hybrid-equilibrium elements with control of spurious kinematic modes* Computer Assisted Mechanics and Engineering Sciences, Volume 4, 1997.

[5] D. Boffi, F. Brezzi, M. Fortin, *Mixed Finite Element Methods and Applications*, Springer, ISBN 978-3-642-36519-5.

[6] F. Vermolen, D. Lahaye, *Building Virtual Models in Engineering*, An Introduction to Finite Elements, Delft University of Applied Mathematics, November 2011.

[7] D. N. Arnold, *Mixed Finite Element Methods for Elliptic problems*, Computer Methods in Applied Mechanics and Engineering, Volume 82, Issues 1–3, September 1990, Pages 281-300.

[8] D.N. Arnold, R.S. Falk, R. Winther, *Finite element exterior calculus: from Hodge theory to numerical stability*, American Mathematical Society, Volume 47, Number 2, April 2010, Pages 281-354.

[9] K. Olsen, B. Gervang, J. N. Reddy, M. Gerritsma, *A Higher Order Equilibrium Finite Element Method*, International Journal for Numerical Methods in Engineering, 2017, Published online in Wiley Online Library.

[10] J.E. Mardsen, T. J. R. Hughes, *Mathematical foundations of Elasticity*, Prentice Hall, 1983.

[11] J. P. Moitinho de Almeida, J. A. Texeira de Freitas, *Continuity conditions for Finite Element Analysis of Solids* International Journal for Numerical Methods in Engineering; 1992.

[12] J. P. Moitinho de Almeida, Edward. A. W. Maunder, *Equilibrium Finite Element Formulations* John Wiley & Sons, 2017.

[13] M. Kempeneers, J. F. Debongnie, P. Beckers, *Pure equilibrium tetrahedral finite elements for global global error estimation in dual analysis*, International Journal for Numerical Methods in Engineering, 2010; 81: 513-536.

[14] Edward. A. W. Maunder, *A general formulation of equilibrium macro-elements with control of spurious kinematic modes: the exorcism of an old curse*, International Journal for Numerical Methods in Engineering, 1996; 39: 3175-3194.

[15] Theodore. H. H. Pian, Chang-Chun Wu, *Hybrid and Incompatible Finite Element Methods* CRC Series: Modern Mechanics and Mathematics, Published in 2006.

[16] Phillip. L. Gould, *Introduction to Linear Elasticity*, Springer, Third edition.

[17] www.brown.edu/Departments/Engineering/Courses/En221/Notes/Conservation_Laws/Conservation_Laws.htm

[18] M.I. Gerritsma, T.N. Phillips, *Compatible Spectral Approximations for the Velocity-Pressure-Stress Formulation of the Stokes problem*, SIAM Journal of Scientific Computing, 1999,20:1530-1550.

[19] https://en.wikipedia.org/wiki/Infinitesimal_strain_theory.

[20] S. Deng, *Quadrature Formulas in 2 Dimensions*, Lecture notes, Math 5172 - Finite Element Method, Section 001, Spring 2010.

[21] P. Solin *Partial Differential Equations and the Finite Element Method*, Appendix A, John Wiley & Sons, Inc

[22] G. E. Karniadakis, S. J. Spencer, *Spectral/hp Element methods for Computational Fluid Dynamics*, Second edition, Oxford Science Publications, 2005.

[23] Charbel Farhat, Francois-Xavier Roux, *A method of finite element tearing and interconnecting and its parallel solution algorithm*, International Journal for Numerical Methods in Engineering, Volume 32, Issue 6, 25 October 1991, Pages 1205–1227.

[24] M. Manolesos, S. G. Voutsinas, *Experimental investigation of the flow past passive vortex generators on an airfoil experiencing three-dimensional separation*, Journal of Wind Engineering & Industrial Aerodynamics, 142, p. 130-148, 2015.

[25] C. Booker, X. Zhang, S. Chernyshenko, *Large-scale source term modelling of vortex generation*, 27th AIAA Applied Aerodynamics Conference, San Antonio, Texas, 2009.

[26] J. C. Dudek, *An Empirical Model for Vane-Type Vortex Generators in a Navier-Stokes Code*, AIAA Journal, Vol. 44, No. 8 (2006), pp. 1779-1789.

[27] N. May, *A new vortex generator model for use in complex configuration CFD solvers*, 19th AIAA Applied Aerodynamics Conference, June 2001.

[28] L. Florentie, S.J. Hulshoff and A.H. van Zuijlen, *Adjoint-based optimization of a source term representation of vortex generators*, submitted to Computers & Fluids, 2017.

[29] *Advanced Variational Methods in Mechanics*, Chapter 1, Variational Calculus Overview, University of Colorado at Boulder.

Appendices

Appendix A

Variational Calculus

Definition A.1. *A functional is a linear mapping from a set of functions to a real number* $\mathbb{R}$.

They are often expressed as definite integrals involving functions and their derivatives. If a and b are known values in $\mathbb{R}^1$, the functional is given by,

$$\mathcal{J}(u) = \int_a^b M(x, u(x), u'(x)) \ dx, \tag{A.1}$$

where $u(x)$ and $M(x, u(x), u'(x))$ are twice continuously differentiable. Writing this as a variational problem in the Hilbert space (Appendix B), we have,

$$\inf_{u \in V} \mathcal{J}(u),$$

which is characterised by the variational equation, [5],

$$\langle \mathcal{J}'(v), u \rangle_{V' \times V} = 0 \qquad \forall u \in V,$$

where $\langle ., . \rangle_{V' \times V}$ denotes duality pairing between vector space V and its dual space V'. Objective functionals often have a linear or quadratic form; making them quite simple to deal with. A block diagram is presented that differentiates between a function and a functional in figure A.1.

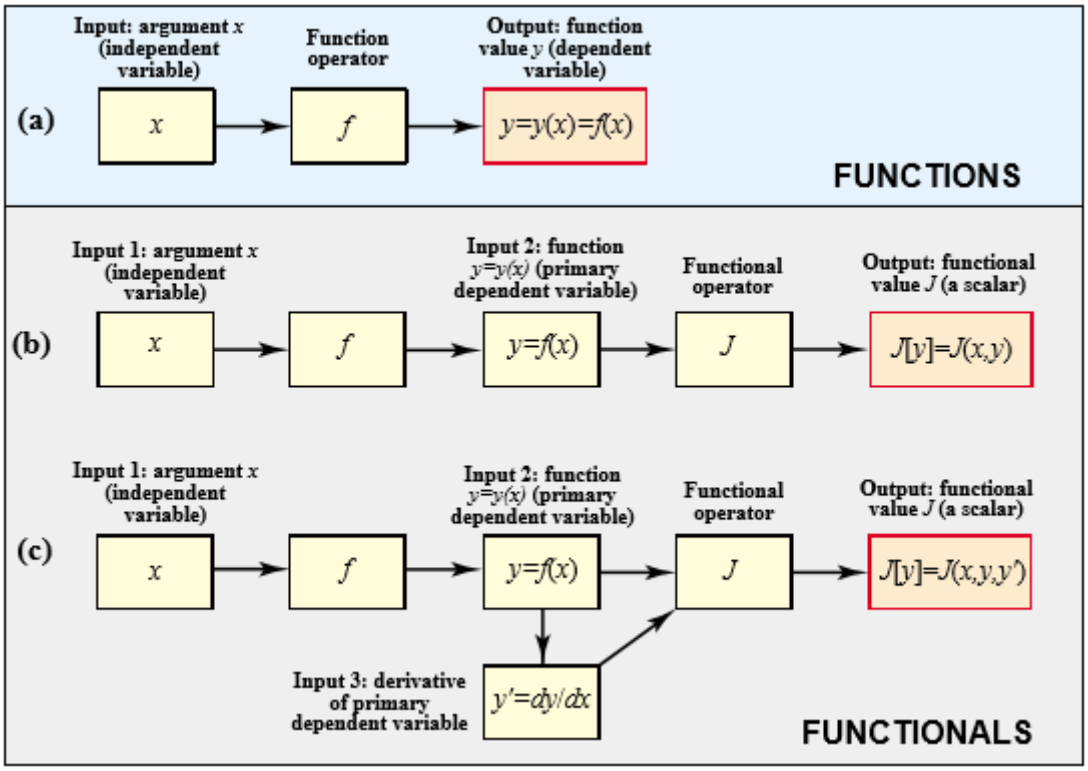

Figure A.1: Simple block diagram for functions and functional, [29]

Definition A.2. *If $x, h \in$ vector space X, then $d\mathcal{J}(x)$ is called the Gâteaux variation of functional $\mathcal{J}$ at x when the limit that is defined as follows exists,*

$$dJ(x,h) = \lim_{\epsilon \to 0} \frac{\mathcal{J}(x+\epsilon h) - \mathcal{J}(x)}{\epsilon} = \frac{d}{d\epsilon}\mathcal{J}(x+\epsilon h)\Big|_{\epsilon=0}.$$

The Gâteaux derivative is the generalisation of the concept of directional derivative in differential calculus. This variation must be equated to 0 for the existence of an extremum for a functional. Gâteaux variations are central to deriving the PDEs from constrained minimisation problems.

Definition A.3. *For a multi-variable differentiable function, a stationary (or critical) point is a point on the surface of the graph where the gradient is zero.*

Definition A.4. *A point of a function or surface which is a stationary point but not an extremum is defined as a saddle point.*

Appendix B

Function spaces

Before introducing Sobolev spaces, we introduce the $L^2(\Omega)$ space consisting of the square integrable functions.

$$L^2(\Omega) \;=\; \left\{ u : \int_\Omega |u|^2 \; d\Omega \;=\; \|u\|^2_{L^2(\Omega)} < \infty \right\}.$$

The Sobolev space of order m (any integer ≥ 0), denoted by $H^m(\Omega)$ is a space of functions and their *weak* partial derivatives upto order m belonging to $L^2(\Omega)$,

$$H^m(\Omega) \;=\; \left\{ u : D^\alpha u \in L^2(\Omega), \forall |\alpha| \leq m \right\}, \tag{B.1}$$

where,

$$D^\alpha u \;=\; \frac{\partial^{|\alpha|} u}{\partial x_1^{\alpha_1} \dots \partial x_n^{\alpha_n}}, \;\; |\alpha| = \alpha_1 + \cdots + \alpha_n,$$

are the weak derivatives, [2]. This type of Sobolev space is a Hilbert space, [21]. Substituting $m = 0$ shows that $H^0(\Omega) = L^2(\Omega)$. For $m = 1$,

$$H^1(\Omega) \;\equiv\; H(\text{grad}; \Omega) \;=\; \left\{ u : u \in L^2(\Omega), \nabla u \in L^2(\Omega) \right\}, \tag{B.2}$$

$H(\text{grad}; \Omega)$.

Another useful result is,

$$\|u\|_{H^m}^2 \;=\; \sum_{|\alpha|\leq m} \|D^\alpha u\|_{L^2}^2.$$

If $m = 2$, and $u \in H^2(\Omega)$ with $\Omega \subset \mathbb{R}^2$,

$$\|u\|_{H^2}^2 \;=\; \int_\Omega u^2 + \left(\frac{\partial u}{\partial x}\right)^2 + \left(\frac{\partial u}{\partial y}\right)^2 + \left(\frac{\partial^2 u}{\partial x^2}\right)^2 + \left(\frac{\partial^2 u}{\partial y^2}\right)^2 + \left(\frac{\partial^2 u}{\partial x \partial y}\right)^2 d\Omega \;<\; \infty,$$

a space that is often used in fourth order elliptic problems. For mixed finite element problems, the following spaces are significant:

$$H(\mathrm{div};\Omega) \;=\; \left\{u : u \in L^2(\Omega),\;\; \nabla \cdot u \in L^2(\Omega)\right\}.$$

$$H_0^1(\Omega) \;=\; \left\{u : u \in H^1(\Omega),\;\; u|_\Gamma = 0\right\}.$$

$$H_0^2(\Omega) \;=\; \left\{u : u \in H^2(\Omega),\;\; u|_\Gamma = 0,\;\; \left.\tfrac{\partial u}{\partial n}\right|_\Gamma = 0\right\}.$$